

# Electrochemical and spectroelectrochemical studies of C-benzodiazaboroly-*ortho*-carboranes

Lothar Weber<sup>\*,a</sup>, Jan Kahlert<sup>a</sup>, Lena Böhling<sup>a</sup>, Andreas Brockhinke<sup>a</sup>, Hans-Georg Stammler<sup>a</sup>, Beate Neumann<sup>a</sup>, Rachel A. Harder<sup>b</sup>, Paul J. Low<sup>b</sup> and Mark A. Fox<sup>\*,b</sup>

<sup>a</sup> Fakultät für Chemie der Universität Bielefeld, 33615 Bielefeld, Germany  
E-mail: lothar.weber@uni-bielefeld.de

<sup>b</sup> Department of Chemistry, Durham University, Durham DH1 3LE, United Kingdom  
E-mail: m.a.fox@durham.ac.uk

† Electronic Supplementary Information (ESI) available: Synthetic procedures and characterisation data for **8,9,11-15,18-21,27,30** and **31**, figures of NMR spectra for **8-15**, crystallographic data and additional structural data, additional photophysical data including absorption and emission spectra for **8-15**, additional computed structural data, simulated IR spectra for **3-5**. See DOI:

## Abstract

Fifteen C-diazaboroly-*ortho*-carboranes, 1-R'-2-R''-1,2-C<sub>2</sub>B<sub>10</sub>H<sub>10</sub>, where R' represents the groups 2-(1,3-Et<sub>2</sub>-1,3,2-N<sub>2</sub>BC<sub>6</sub>H<sub>4</sub>)-, 2-(1,3-Ph<sub>2</sub>-1,3,2-N<sub>2</sub>BC<sub>6</sub>H<sub>4</sub>)-, 2-(1,3-Ph<sub>2</sub>-5,6-Me<sub>2</sub>-1,3,2-N<sub>2</sub>BC<sub>6</sub>H<sub>2</sub>)-, 2-(1,3-<sup>i</sup>Pr<sub>2</sub>-1,3,2-N<sub>2</sub>BC<sub>6</sub>H<sub>4</sub>)-, and 2-(1,3,2-N<sub>2</sub>BC<sub>6</sub>H<sub>6</sub>)- and where R'' equals to H, Me, Ph, <sup>t</sup>Bu or SiMe<sub>3</sub> were synthesized. Cyclovoltammetric studies of the compounds showed irreversible oxidation waves which are caused by the oxidation of the heterocycle. Those C-diazaboroly-*ortho*-carboranes with Ph, <sup>t</sup>Bu SiMe<sub>3</sub> substituents at the adjacent C-atom of the cage displayed two one-electron reduction waves reflecting the formation of stable radical monoanions with unusual (2n+3) skeletal electron counts. The geometries of these anions were determined by combinations of infrared, UV-visible spectroelectrochemical and computational studies. Additionally the structures of seven new C-diazaboroly-*ortho*-carboranes and one new 2-bromo-1,3,2-benzodiazaborole were determined by X-ray crystallography and compared with previously obtained structures.

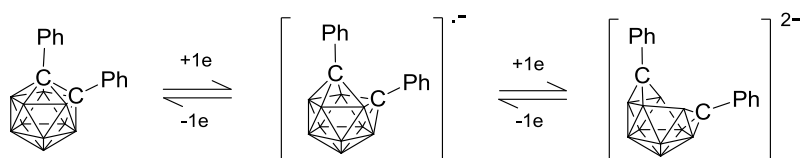
## Introduction

Although numerous carborane clusters have been known for fifty years,<sup>1,2</sup> efforts to understand their unique electronic properties are still continuing. The most widely studied carborane 1,2-C<sub>2</sub>B<sub>10</sub>H<sub>12</sub>, *ortho*-carborane, displays a rich chemistry.<sup>1</sup> Because of the electron deficient character of this icosahedral cage its C-H bonds are activated and thus prone to deprotonation and substitution processes.

As a *closo*-cluster, 1,2-C<sub>2</sub>B<sub>10</sub>H<sub>12</sub> possesses 26 skeletal electrons, or 2n+2 skeletal electrons according to Wade's electron-counting rules (n = number of cluster atoms).<sup>3</sup> This molecule readily accommodates two additional electrons to form a dianion with 28 skeletal electrons (2n+4) and a more open *nido*-structure.<sup>4</sup> Electrochemical studies on the parent *ortho*-carborane revealed an irreversible two-electron reduction which is

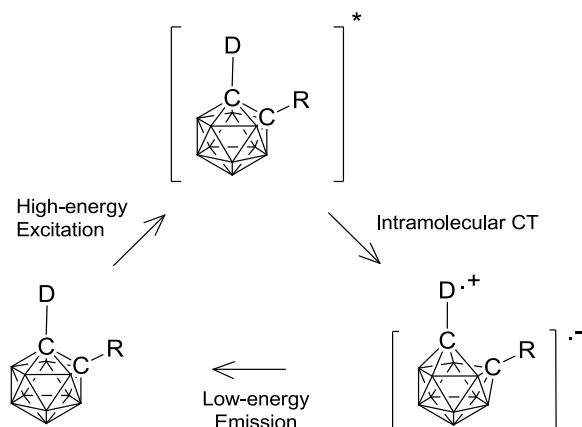
rationalized by a facile CH-cleavage and the subsequent reaction of the transient anion  $C_2B_{10}H_{11}^-$  with a second molecule of 1,2- $C_2B_{10}H_{12}$  to afford the two-cage anion [*closo*- $C_2B_{10}H_{11}$ -*nido*- $C_2B_{10}H_{12}$ ].<sup>5,6</sup>

Logically, *ortho*-carboranes with two substituents at the adjacent C-atoms should be electrochemically more robust. Cyclovoltammetric investigations on the 1,2-diphenyl-derivative showed two one-electron reduction waves which are taken as evidence for the occurrence of a stable radical anion.<sup>7</sup> More recently, the geometry of the radical anion was elucidated by means of IR- and UV- spectroelectrochemical, ESR and computational methods<sup>8</sup> (Scheme 1).



Scheme 1. Two one-electron reductions for 1,2-diphenyl-*ortho*-carborane.

According to computations, the additional electron is located at the cage atoms giving rise to an elongated C-C distance of 2.39 Å in comparison to the neutral precursor (1.76 Å). With regard to the many *closo*- and *nido*- carboranes, carborane-based radical anions featuring a  $2n+3$  electron count are somewhat rare.<sup>8-13</sup> In a more recent report on the photophysics of *ortho*-carboranes with donating arylcarbazolyl substituents it was suggested that the species in their excited states consist of carbazolyl radical cations and radical cluster anions. This assumption was based on absorption spectroscopy where a transient band at 415 nm with a similar spectral profile as the corresponding radical anion was observed<sup>13</sup> (Scheme 2). There are many reports of unusual low-energy emissions from 1-mono- and 1,2-di-aryl-*ortho*-carboranes which are explained by charge-transfer between the electron-accepting *ortho*-carborane and the electron-donating aryl groups.<sup>14,15</sup>



Scheme 2. Excited state geometries for *ortho*-carboranes proposed to explain low-energy emissions observed experimentally. D represents a donor group.

We recently reported<sup>16</sup> on the synthesis and photophysical behaviour of a number of *ortho*-carboranes (**1-7**, Chart I) featuring a 1,3-diethyl- and 1,3-diphenyl-1,3,2-

benzodiazaborolyl substituent at one cage carbon atoms. Apart from **6**, these compounds show remarkable low-energy fluorescence emissions with Stokes shifts of 15100-20260  $\text{cm}^{-1}$  and quantum yields up to 65% in the solid state. These low-energy emissions are due to a charge transfer between the electron-accepting cage and the electron-donating benzodiazaborolyl unit.

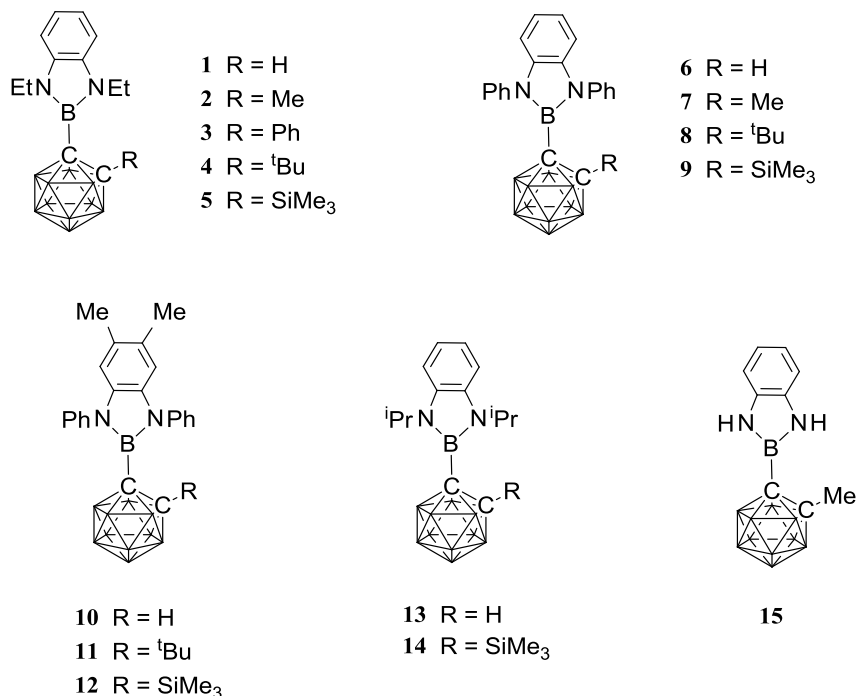
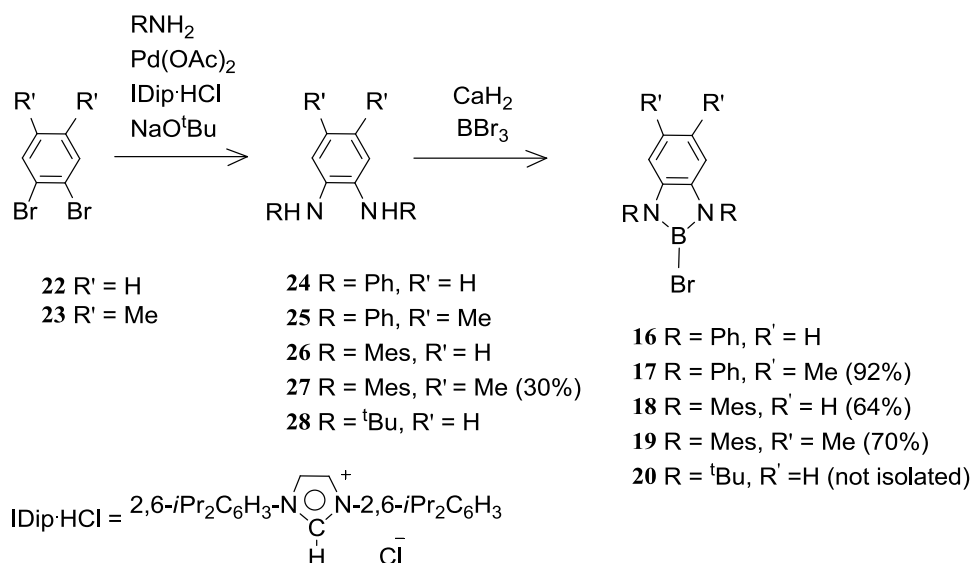


## Chart I

Here we describe the syntheses, structural, photophysical and computational studies for the eight new C-diazaborolylcarboranes, **8-15** (Chart I). More importantly, electrochemical and spectroelectrochemical studies disclose carborane radical anions on reductions of some diazaborolyl-*ortho*-carboranes. This study shows that unusual  $2n+3$  carborane radical anions were formed with bulky *tert*-butyl and trimethylsilyl substituents in addition to aryl groups at the adjacent cage carbon.

## Syntheses

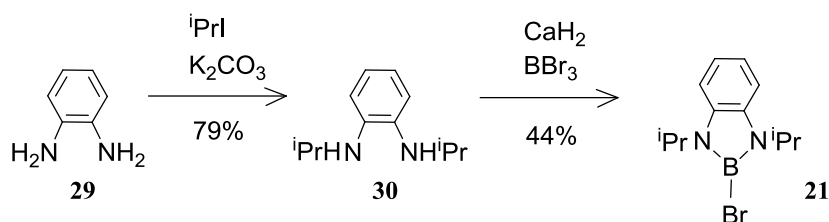
In our group the 2-bromo-1,3,2-benzodiazaborole 2-Br-1,3-Et<sub>2</sub>-1,3,2-N<sub>2</sub>BC<sub>6</sub>H<sub>4</sub><sup>17</sup> has been frequently used as a precursor for many fluorescent benzodiazaboroles<sup>18-22</sup> including carboranes **1-5** (Chart I). Analogously, 2-Br-1,3-Ph<sub>2</sub>-1,3,2-N<sub>2</sub>BC<sub>6</sub>H<sub>4</sub> (**16**)<sup>19</sup> (Scheme 3) was utilized as a starting material for benzodiazaborole dyes such as **6** and **7**.<sup>16</sup> The protocol for **16** was extended for the preparation of the novel compounds **17-18** having phenyl or mesityl rings at the N-atoms and hydrogen or methyl substituents at the six-membered ring (Scheme 3).



Scheme 3. Syntheses of bromodiazaboroles from 1,2-dibromobenzenes (yields of new compounds in parentheses).

Surprisingly the corresponding reaction of **28**, featuring two *N-tert*-butyl groups, with  $\text{BBr}_3$  failed. The  $^{11}\text{B}\{^1\text{H}\}$  NMR spectrum of the reaction mixture was characterized by a broad hump at 25 ppm and a less intense signal at 22 ppm which were presumably due to oligomeric triaminoboranes and 2-bromobenzodiazaboroles (including **20**), respectively. The known cyclic  $\text{B}_3\text{N}_3$  trimer ( $\text{C}_6\text{H}_4\text{NHBN}$ ) $_3$ <sup>23</sup> was identified in the reaction mixture by mass spectroscopy.

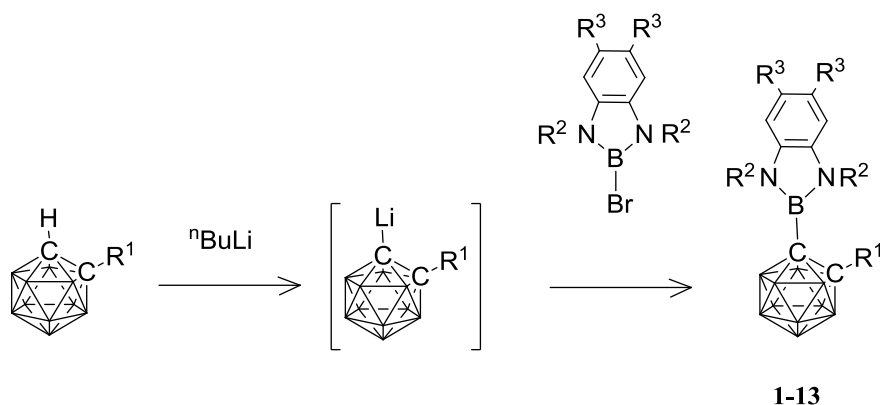
The synthesis of 2-bromo-1,3-di-*iso*-propylbenzodiazaborole (**21**)<sup>24</sup> required the *N,N'*-di-*iso*-propylphenylene diamine (**30**), which, deviating from the literature, was obtained by a facile multigram procedure from 1,2-phenylene diamine and 2-iodopropane in the presence of  $\text{K}_2\text{CO}_3$  (79% yield, Scheme 4).



Scheme 4. Synthesis of bromoborole **21**.

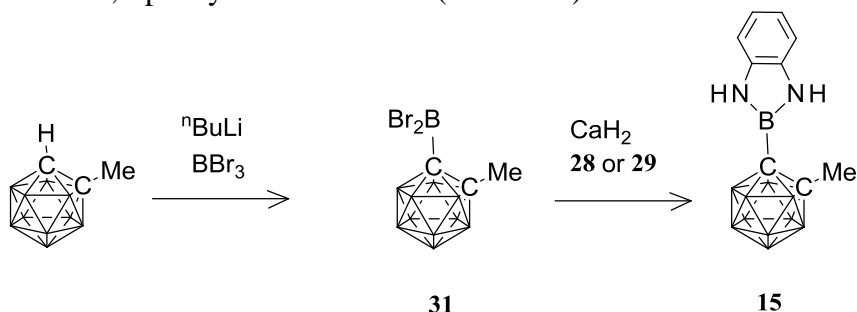
The standard protocol for C-monodiazaborolyl carboranes is based on the treatment of the lithiated carborane with bromodiazaboroles as depicted in Scheme 5. Thus, the reactions of bromodiazaboroles **16**, **17** and **21** with the corresponding lithiated carborane afforded the carboranes **8-13**.

Attempts to form C-diazaborolylcarboranes with the bromodiazaboroles **18** and **19** containing bulky mesityl groups were not successful. The trimethylsilylcarborane **14** was obtained from lithiation of **13** followed by addition of  $\text{Me}_3\text{SiCl}$ .



Scheme 5. General route to C-monodiazaborolylo-*ortho*-carboranes, **1-13**.

Due to the failure of the synthesis of 2-bromobenzodiazaborole **20** a protocol according to Scheme 5 for a C-diazaborolylo carborane with two bulky *tert*-butyl groups at the N-atoms had to be discarded. Thus an alternative route via a base assisted cyclocondensation of phenylene diamine **28** with 1-dibromo-2-methyl-*ortho*-carborane **31** was envisaged. Compound **31** resulted from the metalation of 1-methyl-*ortho*-carborane by *n*-butyllithium in toluene and the subsequent addition of BBr<sub>3</sub> to the lithio-carborane at -90°C. The low temperature during the addition of BBr<sub>3</sub> was crucial to avoid an intractable product mixture. Short path distillation afforded pure **31** as a colourless oil in 67 % yield. For further transformations this material was, however, employed *in situ*. Thus, reaction with **28** afforded diazaborolylo carborane **15** in 25% isolated yield. Obviously the *tert*-butyl groups were liberated during the cyclocondensation. In keeping with this the yield of **15** can be improved to 46% by reacting **31** with 1,2-phenylene diamine **29** (Scheme 6).



Scheme 6. Synthesis of carborane **15** via the dibromoborylo-*ortho*-carborane **31**.

<sup>1</sup>H, <sup>11</sup>B and <sup>13</sup>C NMR spectra for all new carboranes **8-15** are depicted in Figures S1-S24. Of interest are the two distinct methyl group resonances observed in the <sup>1</sup>H and <sup>13</sup>C NMR spectra of compound **14**, pointing to a restricted rotation of the <sup>1</sup>Pr groups due to the silyl group. Similarly, two sets of <sup>1</sup>H and <sup>13</sup>C NMR signals for the *ortho*-positions in the N-phenyl rings in **8**, **9**, **11** and **12** are indicative for the hindered rotations of the diazaborolylo group and the phenyl groups.

### X-ray Crystallography

Molecular structures were determined for the 1-diazaborolylo-*ortho*-carboranes, **8-13** and **15** (Figure 1). Table 1 lists selected bonding parameters for these compounds in

comparison to the data previously reported<sup>16</sup> for **1-7** including the torsion angles C2-C1-B2-N3 ( $\psi$ ) and the aryl-borolyl interplanar angles ( $\omega$ ) shown in Figure 2. The carborane C1-C2 bond length increases with more steric bulk of the substituent at C2, in the series **1-13** going from 1.656-1.670 Å for H, 1.684-1.686 Å for Me, 1.707-1.719 Å for SiMe<sub>3</sub> and 1.701-1.730 Å for Ph to 1.738-1.756 Å for <sup>t</sup>Bu. Compound **15** with a methyl substituent at C2 has a shorter C1-C2 bond (1.669 Å) than the similar carboranes **2** and **7** due to the lack of substituents at the nitrogen atoms of the diazaborolyl group.

Each of the four compounds **1**, **6**, **10** and **13** has a hydrogen atom attached to C2, which may cause cage disorders in the crystal in the absence of C-H...X interactions.<sup>25</sup> Indeed, there are such C-H... $\pi$  interactions in **1**, **6** and **10** but not in the di-*iso*-propyl derivative **13**. The latter compound contains two independent molecules in the asymmetric unit, one of which has a disordered cage. The data of the ordered molecule of **13** are listed in Table 1.

In the crystal of compound **4**, the *tert*-butyl group is disordered over two positions with torsion angles C1-C2-C22-C23 ( $\theta$ , Figure 2) of 8.9° (conformer **4A** with one methyl group almost co-planar with the C1-C2 bond) and 43.0° (conformer **4B**) with 77:23 occupancies.<sup>16</sup> The *tert*-butyl groups in **8** and **11** are not disordered and show torsion angles  $\theta$  of 17.3° and 21.1°, respectively.

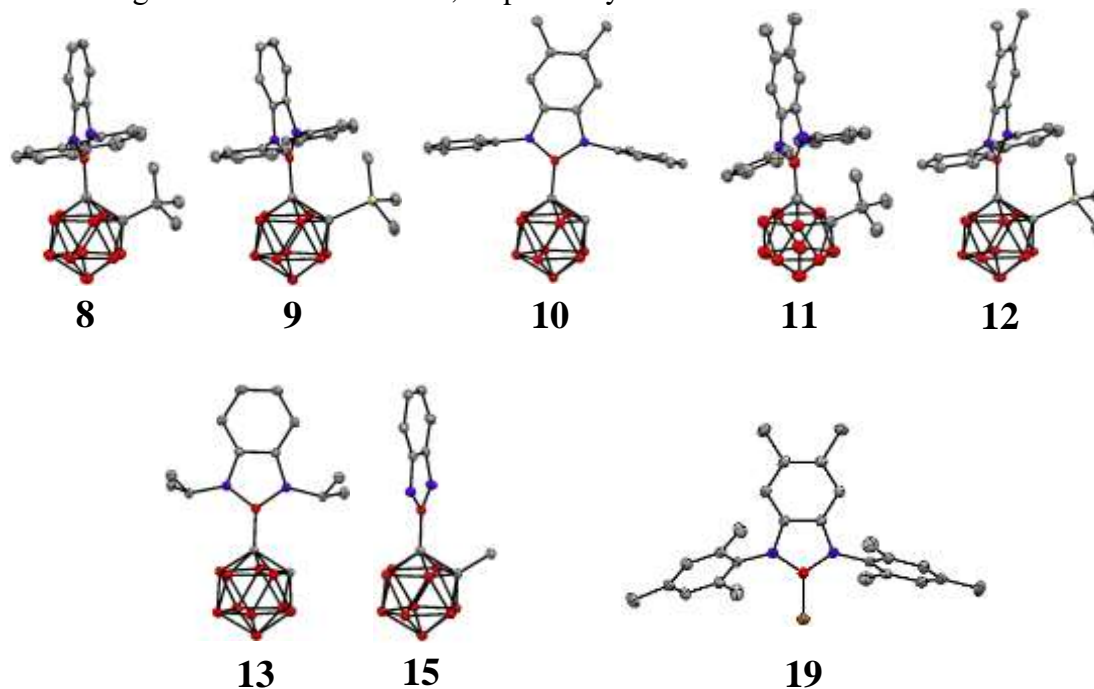


Figure 1. Molecular structures of compounds **8-13**, **15** and **19**. All hydrogen atoms are omitted for clarity.

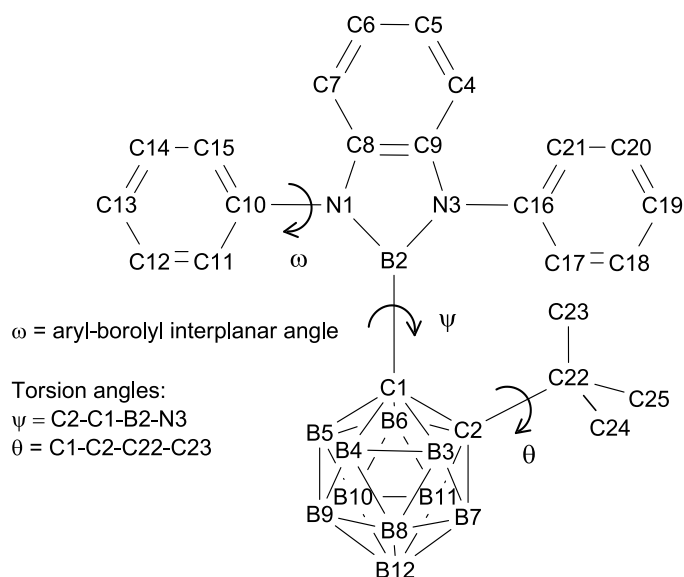


Figure 2. Atom labelling of 1-(1',3'-diphenylbenzodiazaborolyl)-2-*tert*-butyl-*ortho*-carborane (**8**) with pertinent torsion angles ( $\psi$ ,  $\theta$ ) and interplanar angle  $\omega$ .

Table 1. Selected bond lengths and angles of 1-benzodiazaborolyl-*ortho*-carboranes **1-13** and **15**.

	Substituents <sup>[a]</sup>			Bond lengths [Å]		Angles [°]	
	R <sup>1</sup>	R <sup>2</sup>	R <sup>3</sup>	C1-B2	C1-C2	ψ	ω
<b>1</b>	H	Et	H	1.594(2)	1.670(1)	92.4	-
<b>2</b>	Me	Et	H	1.605(3)	1.684(2)	88.8	-
<b>3</b>	Ph	Et	H	1.600(3)	1.687(2)	89.8	-
				1.600(2)	1.730(2)	89.3	
				1.609(2)	1.720(2)	86.6	
<b>4</b>	<sup>t</sup> Bu	Et	H	1.606(1)	1.701(2)	67.5	-
				1.606(1)	1.756(1)	89.6	
				1.605(1)	1.710(1)	83.7	
<b>5</b>	SiMe <sub>3</sub>	Et	H	1.605(1)	1.710(1)	83.7	-
<b>6</b>	H	Ph	H	1.586(2)	1.670(2)	16.6	75.8/76.4
<b>7</b>	Me	Ph	H	1.591(2)	1.686(2)	80.0	72.2/76.5
<b>8</b>	<sup>t</sup> Bu	Ph	H	1.595(2)	1.750(2)	82.9	77.2/89.0
<b>9</b>	SiMe <sub>3</sub>	Ph	H	1.595(2)	1.707(2)	79.6	84.0/83.2
<b>10</b>	H	Ph	Me	1.585(2)	1.656(1)	12.2	67.8/80.2
				1.597(3)	1.743(3)	87.3	83.2/83.8
<b>11</b>	<sup>t</sup> Bu	Ph	Me	1.595(3)	1.738(3)	85.9	84.1/76.1
				1.594(2)	1.719(2)	79.2	64.5/77.8
<b>12</b>	SiMe <sub>3</sub>	Ph	Me	1.594(2)	1.719(2)	79.2	64.5/77.8
<b>13</b>	H	<sup>i</sup> Pr	H	1.604(2)	1.664(1)	12.2	-
<b>15</b>	Me	H	H	1.580(1)	1.669(1)	77.7	-

[a] see Scheme 5.

The four independent molecules in the unit cell of bromobenzodiazaborole **19** show mesityl groups which are nearly orthogonally oriented to the plane of the heterocycle with interplanar angles ( $\omega$ ) between 75.2 and 87.5° (Table S1). These values are similar to the interplanar angles  $\omega$  observed in the molecular structures for compounds

**6-12** shown in Table 1. The B-Br bond lengths of 1.909(2)-1.915(2) Å in **19** are slightly shorter than the B-Br distance of 1.925(5) Å in the only other structurally characterized bromobenzodiazaborole, 1,4-[1'-(2'-Br-3'-<sup>i</sup>Pr-1',3',2'-N<sub>2</sub>BC<sub>6</sub>H<sub>4</sub>)]<sub>2</sub>C<sub>6</sub>H<sub>4</sub>.<sup>20</sup>

The bonding parameters within the benzodiazaborole units were similar to those of other previously reported structures.<sup>16,18-21</sup> The carborane C1 -borolyl B bond lengths increases from 1.580 Å in **15** with NH groups via 1.586-1.597 Å with NPh substituents to 1.594-1.609 Å with N-alkyl groups reflecting the increased bulk of the substituents.

## Photophysics

Absorption data for the 1-benzodiazaborolyl-*ortho*-carboranes **8-15** in cyclohexane, toluene, chloroform and dichloromethane solutions and also as solids are listed in **Table S3** and shown in Figures S25-S32. Like for **1-7**,<sup>16</sup> all highest energy absorption maxima were observed in the 294-303 nm region. These absorptions are assigned to local  $\pi$  to  $\pi^*$  transitions at the diazaborolyl groups.

Table 2 lists the emission data for **8-15** in cyclohexane and dichloromethane solutions and as solids along with data for **1-7** for comparison. Additional emission data for **8-15** in other solvents are listed in **Tables S4-S7** and the respective spectra are shown in Figures S25-S32. In cyclohexane solutions, low-energy emissions with maxima between 534 nm (for **7**) and 620 nm (for **14**) were observed for all carboranes except for **6** and **10**. These emissions are assigned to a charge-transfer (CT) from the cluster to the benzodiazaborolyl group. Notably, the emission maxima of 1,3-diphenylbenzodiazaboroles **8** and **9** are blue-shifted by 36-45 nm compared to their 1,3-diethyl- and 5,6-dimethyl-1,3-diphenyl analogues **4**, **5**, **11** and **12**. This underlines that the CT state is better stabilized by the more electron-rich benzodiazaborolyl groups. High-energy emissions between 302 nm and 346 nm were present for **1**, **6**, **7** and **10** and are attributed to local  $\pi^*$  to  $\pi$  transitions at the diazaborolyl groups. The quantum yields of the low energy emission ( $\Phi^F$ ) depend on the substituent R<sup>1</sup> (Scheme 5) at carbon C2 of **1-14** with values of 1% or less for R<sup>1</sup> = H, up to 8% for Me, 6% for Ph, 14-45% for SiMe<sub>3</sub> and 32-38% for <sup>t</sup>Bu. Thus, the new C-diazaborolyl-carboranes confirm the idea that bulky substituents at C2 increase the quantum yields by restriction of intramolecular rotations.

In the more polar solvent dichloromethane, low-energy emissions were detected for all carboranes except **6**, **10** and **15**. The emission maxima in dichloromethane were red-shifted with respect to those observed in cyclohexane. The transition dipole moments estimated by use of the Lippert-Mataga method with an Onsager radius of 3.52 Å range from 6.9 to 10.9 D reflecting the CT nature of these emissions. The quantum yields were generally much lower in dichloromethane solutions, with the highest value of  $\Phi^F$  = 6% for **8**, when compared with those in cyclohexane solutions.

Coloured emission can be seen with the naked eye, when crystals of **8**, **9**, **11**, **12**, **14** and **15** are irradiated by UV-light (Figure 3). Compound **13** gives a faint yellow emission under UV irradiation which was not bright enough to be photographed. The solid state emission data are listed in Table 2 whereby the quantum yields reflect the brightness of the colours in Figure 3. The relationship between the borolyl orientation described by  $\psi$  in the crystals and the low-energy CT emissions previously postulated for **1-7** is reinforced for the new carboranes **8-13** and **15**. The two compounds **6** and **10** which do not emit in the solid state contain the borolyl units in near co-planar

orientation with the C1-C2 bond featuring small  $\psi$  angles of  $16.6^\circ$  and  $12.2^\circ$ , respectively. Increased  $\psi$  angles between  $67.5^\circ$  and  $92.4^\circ$  were found for **1-5**, **7-9**, **11-13** and **15** with  $\Phi^F$  values between 25 and 70%.

Carborane **13** has one molecule in the asymmetric unit with  $\psi = 12.2^\circ$  so it would not be expected to emit in the solid state but the second molecule probably contains conformers with higher  $\psi$  angles as the cluster in the latter molecule is disordered. These conformers are presumably responsible for the relatively weak low energy emission with  $\Phi^F = 5\%$  observed in the solid state.

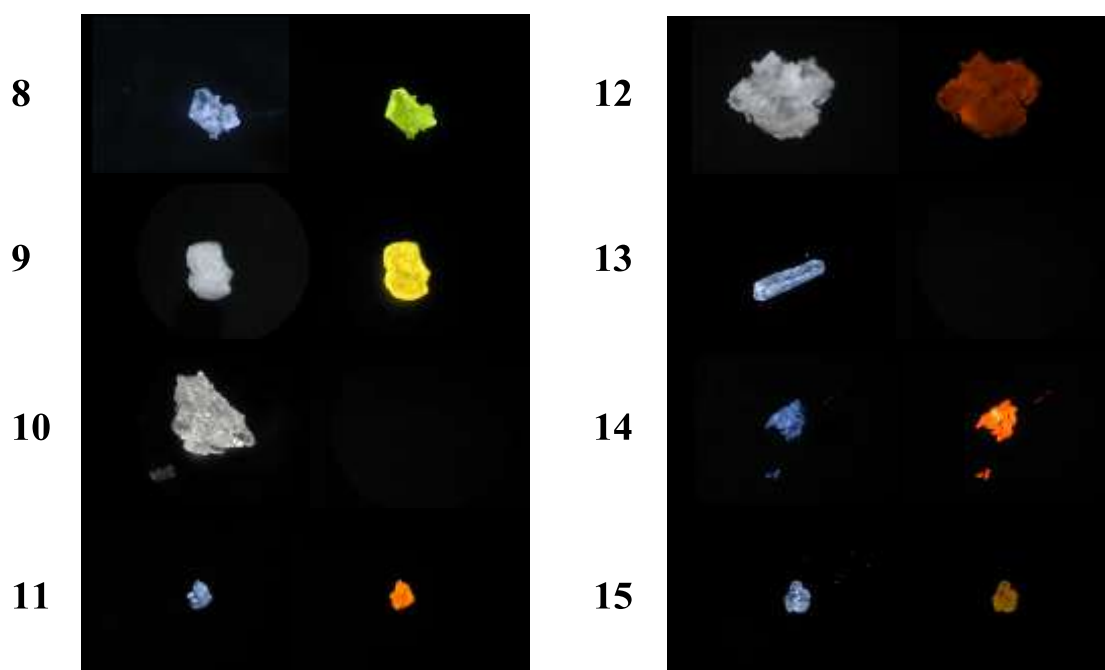


Figure 3. Left columns: Crystals of compounds **8-15** without UV irradiation. Right columns: Under UV irradiation at 350 nm.

Table 2. Emission data of **1** - **15**.

	R <sup>1</sup>	R <sup>2</sup>	R <sup>3</sup>	Emission $\lambda_{\max}$ [nm] in cyclohexane	Stokes shift [cm <sup>-1</sup> ] in cyclohexane	$\Phi_F$ [%] in cyclohexane	Emission $\lambda_{\max}$ [nm] in DCM	Stokes- shift [cm <sup>-1</sup> ] in DCM	$\Phi_F$ [%] in DCM	Emission $\lambda_{\max}$ [nm] in solid state	Stokes shift [cm <sup>-1</sup> ] in solid state	$\Phi_F$ [%] in solid state <sup>[a]</sup>	Transition dipole moment <sup>[b]</sup> [D]
<b>1</b>	H	Et	H	311, 596	1960, 15660	< 1	720	19030	< 1	561	16060	51	8.4
<b>2</b>	Me	Et	H	574	16480	8	692	19800	3	573	16520	65	8.1
<b>3</b>	Ph	Et	H	615	18050	6	757	21340	1	613	15100	30	8.3
<b>4</b>	<sup>t</sup> Bu	Et	H	587	17420	32	713	20330	3	611	16160	42	7.6
<b>5</b>	Me <sub>3</sub> Si	Et	H	602	18090	18	726	20870	2	631	20260	30	7.4
<b>6</b>	H	Ph	H	302, 346	1850, 6600	1	417	11170	< 1	- <sup>[c]</sup>	-	-	-
<b>7</b>	Me	Ph	H	345, 534	5540, 15880	< 1	646	19200	< 1	523	15340	25	8.0
<b>8</b>	<sup>t</sup> Bu	Ph	H	548	16510	38	665	19560	6	557	17030	70	7.7
<b>9</b>	Me <sub>3</sub> Si	Ph	H	557	16920	40	669	19890	3	573	15620	58	7.6
<b>10</b>	H	Ph	Me	314	1840	< 1	317	2010	< 1	- <sup>[c]</sup>	-	-	-
<b>11</b>	<sup>t</sup> Bu	Ph	Me	584	16420	33	720	19680	2	606	16550	55	8.4
<b>12</b>	Me <sub>3</sub> Si	Ph	Me	598	14120	45	733	20150	1	621	14590	27	10.9
<b>13</b>	H	<sup>i</sup> Pr	H	616	18560	1	744	21030	< 1	654	17270	5	6.9
<b>14</b>	Me <sub>3</sub> Si	<sup>i</sup> Pr	H	620	18320	14	739	20740	1	627	16200	58	6.9
<b>15</b>	Me	H	H	551	17300	< 1	- <sup>[d]</sup>	-	-	595	16460	33	- <sup>[e]</sup>

[a] Measured by using an integrating sphere method.

[b] From low energy emission data.

[c] Not emissive in the solid state.

[d] Decomposes in DCM.

[e] Not enough data for a Lippert-Mataga plot.

## Electrochemistry

Cyclovoltammetric data on **1-15** with a platinum working electrode in dichloromethane are summarised in Table 3. CV traces for the reduction waves of the disubstituted carboranes **3**, **4** and **5** are depicted in Figure 4. These poorly resolved CV waves are typical for disubstituted carboranes as shown elsewhere<sup>15,26</sup> including diaryl-*ortho*-carboranes.<sup>8,10-13</sup> CV traces for the phenyl (**3**) and trimethylsilyl (**5**) derivatives show cathodic waves indicating a two-electron reduction and anodic waves corresponding to two one-electron oxidations after reduction. The CV trace for the *tert*-butyl derivative **4**, however, subtly reveals two one-electron waves on reduction rather than one two-electron reduction. The electron transfer rate for the second one-electron reduction is faster than the first one-electron reduction. The slow electron transfer with the first reduction may be related to a considerable geometric rearrangement taking place. Similar CV traces as for **4** and **5** are observed for the other *tert*-butyl and trimethylsilyl derivatives, **8**, **9**, **11**, **12** and **14** with data listed in Table 3.

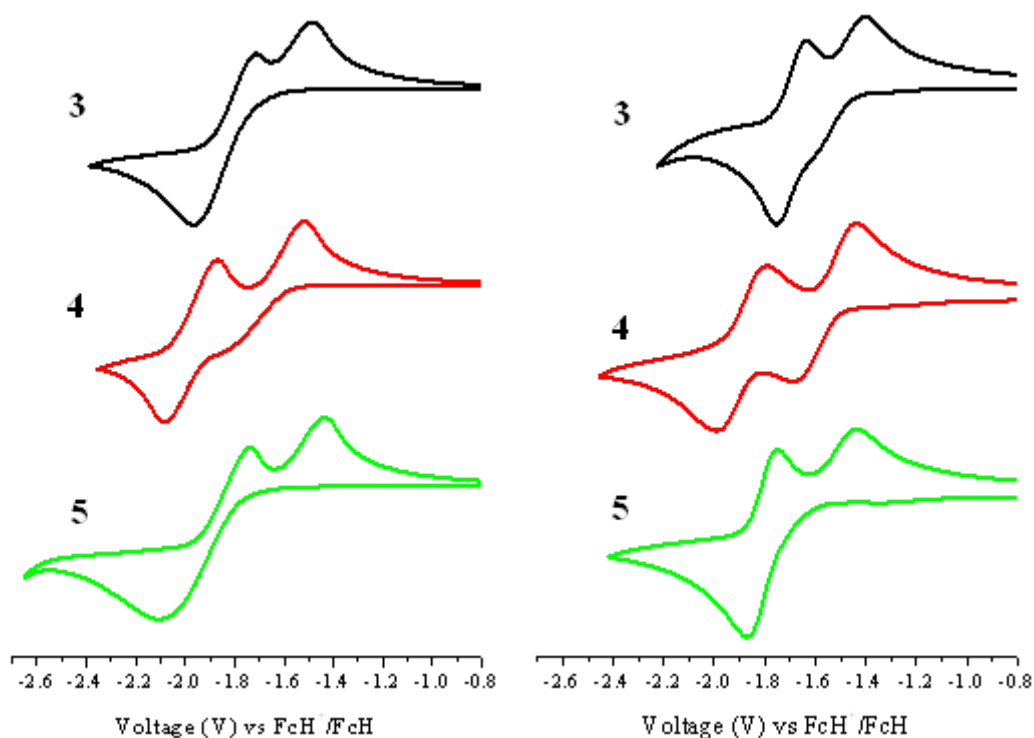


Figure 4. Cyclovoltammetry traces for reductions of **3**, **4** and **5** in dichloromethane (left) and in acetonitrile (right) solutions.

Table 3. Cyclovoltammetric data for **1-15** with a platinum working electrode in dichloromethane and a scan rate of 100mV/s.

	R <sup>1</sup>	R <sup>2</sup>	R <sup>3</sup>	E <sup>a</sup> (Ox) V <sup>[a]</sup>	E <sup>c</sup> (Red1) V <sup>[b]</sup>	E <sup>a</sup> (Red1) V	E <sub>1/2</sub> (Red1) V	E <sup>a</sup> -E <sup>c</sup> (Red1) mV	E <sup>c</sup> (Red2) V	E <sup>a</sup> (Red2) V	E <sub>1/2</sub> (Red2) V	E <sup>a</sup> -E <sup>c</sup> (Red2) mV	ΔE <sub>1/2</sub> (Red1-Red2) mV
<b>1</b>	H	Et	H	0.92									
<b>2</b>	Me	Et	H	<i>1.2</i>									
<b>3</b>	Ph	Et	H	0.97	-1.92	-1.54	-1.73	380	-1.92	-1.77	-1.85	150	120
<b>4</b>	<sup>t</sup> Bu	Et	H	1.04	-2.03	-1.57	-1.80	460	-2.03	-1.92	-1.98	110	180
<b>5</b>	Me <sub>3</sub> Si	Et	H	1.09	-2.06	-1.50	-1.78	560	-2.06	-1.80	-1.93	260	150
<b>6</b>	H	Ph	H	1.11									
<b>7</b>	Me	Ph	H	<i>1.2</i>									
<b>8</b>	<sup>t</sup> Bu	Ph	H	1.24	-2.26	-1.52	-1.89	740	-2.26	-1.94	-2.10	320	210
<b>9</b>	Me <sub>3</sub> Si	Ph	H	1.19	-2.56	-1.51	-2.04	1050	-2.56	-1.91	-2.24	650	200
<b>10</b>	H	Ph	Me	0.89									
<b>11</b>	<sup>t</sup> Bu	Ph	Me	0.98	-2.27	-1.56	-1.92	710	-2.27	-1.97	-2.12	300	200
<b>12</b>	Me <sub>3</sub> Si	Ph	Me	1.13	-2.62	-1.49	-2.06	1130	-2.62	-1.89	-2.26	730	200
<b>13</b>	H	<sup>i</sup> Pr	H	0.96									
<b>14</b>	Me <sub>3</sub> Si	<sup>i</sup> Pr	H	1.31	-2.29	-1.30	-1.76	990	-2.29	-1.76	-2.03	530	270
<b>15</b>	Me	H	H	1.13									

[a] Irreversible wave, values in italics are from ill-defined waves; [b] No observed reduction waves within the solvent window for **1,2,6,7,10,13** and **15**.

Compounds **1**, **2**, **6**, **7**, **10**, **13** and **15** with hydrogen or methyl groups at C2 do not show reduction waves within the solvent window of dichloromethane. These derivatives are thus more difficult to reduce than the phenyl, *tert*-butyl and silyl derivatives which may be related to the differences in the C1-C2 bond lengths with 1.656-1.687 Å for R<sup>1</sup> = H or Me and 1.701-1.756 Å for R<sup>1</sup> = Ph, <sup>t</sup>Bu or SiMe<sub>3</sub> from X-ray studies (Table 1).

All the benzodiazaborolyl-*ortho*-carboranes here exhibit irreversible oxidation waves with multiple electron oxidations as may be deduced from the intensity of the waves relative to the reduction waves. These irreversible oxidations take place at the electron-donating diazaborolyl group in agreement with other benzodiazaboroles.<sup>21,27</sup> The anodic wave values E<sup>a</sup>(Ox) should be regarded as approximate as these waves are ill-defined.

More defined cyclovoltammetric waves were obtained using a glassy carbon working electrode in acetonitrile as shown in Figure 4 for **3**, **4** and **5**. The CV of the phenyl derivative **3** shows two one-electron cathodic waves on reduction rather than the one two-electron wave found in dichloromethane. The *tert*-butyl compound **4** shows in CH<sub>3</sub>CN clearly defined two one-electron waves whereas the CV of the silyl derivative **5** still displays one two-electron cathodic wave. However, in all compounds the peak-peak separations E<sup>a</sup>-E<sup>c</sup> are smaller in acetonitrile than in dichloromethane. As the peak-peak separations for the internal ferrocenium/ferrocene couples in both solvents are similar it is obvious that the reduction waves of these carboranes are influenced considerably by the solvent used. CV traces like those for **4** and **5** were observed for the other *tert*-butyl and trimethylsilyl derivatives **8**, **9** and **14** (Table 4). Unfortunately, compounds **11** and **12** were insoluble in acetonitrile.

Reduction waves were also observed in acetonitrile solutions for **1**, **2**, **6**, **7**, **10**, **13** and **15** with hydrogen or methyl groups at C2 i.e. R<sup>1</sup> = H or Me (Scheme 5). The cathodic waves occur at reduction potentials E<sup>c</sup> of -2.35 to -2.96 V vs the internal FcH<sup>+</sup>/FcH couple which are more negative than -1.69 to -2.09 V found for the phenyl, butyl and silyl derivatives here. The anodic waves after reductions are at much lower potentials E<sup>a</sup> and of lower intensities than the corresponding cathodic waves for compounds with R<sup>1</sup> = H or Me. Similar CV traces have been reported for 1-methyl-*ortho*-carborane and 1,2-dimethyl-*ortho*-carborane where protonation of the formed dianions was postulated.<sup>7</sup> The dianions generated from diazaborolyl-*ortho*-carboranes with R<sup>1</sup> = H or Me are not stable under these electrochemical conditions. The CV traces of the carboranes are thus better defined in acetonitrile than in dichloromethane, but the compounds slowly decompose in acetonitrile.

Table 4. Cyclovoltammetric data for **1-10** and **13-15** with a glassy carbon working electrode in acetonitrile and scan rate of 100mV/s.

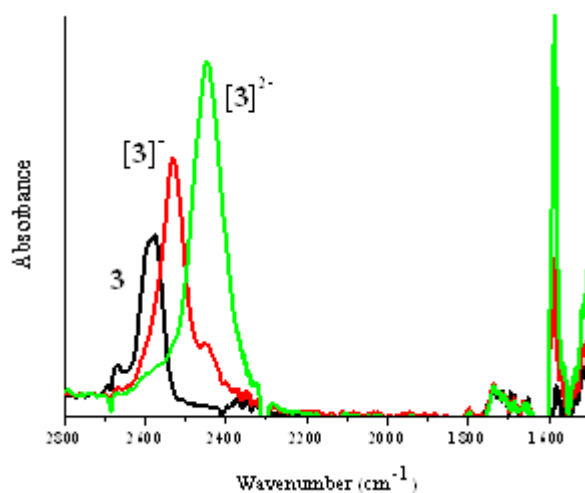
	R <sup>1</sup>	R <sup>2</sup>	R <sup>3</sup>	E <sup>a</sup> (Ox) V <sup>[a]</sup>	E <sup>c</sup> (Red1) V	E <sup>a</sup> (Red1) V <sup>[b]</sup>	E <sub>1/2</sub> (Red1) V	E <sup>a</sup> -E <sup>c</sup> (Red1) mV	E <sup>c</sup> (Red2) V	E <sup>a</sup> (Red2) V <sup>[b]</sup>	E <sub>1/2</sub> (Red2) V	E <sup>a</sup> -E <sup>c</sup> (Red2) mV	ΔE <sub>1/2</sub> (Red1-Red2) mV
<b>1</b>	H	Et	H	0.87	-2.81	<i>-1.50</i>			-2.81	<i>-1.80</i>			
<b>2</b>	Me	Et	H	1.04	-2.35	<i>-1.50</i>			-2.35	<i>-1.76</i>			
<b>3</b>	Ph	Et	H	0.97	-1.76	-1.39	-1.58	370	-1.76	-1.64	-1.70	120	120
<b>4</b>	<sup>t</sup> Bu	Et	H	0.98	-1.69	-1.44	-1.56	260	-1.99	-1.79	-1.89	200	330
<b>5</b>	Me <sub>3</sub> Si	Et	H	1.02	-1.89	-1.41	-1.65	480	-1.89	-1.75	-1.82	140	170
<b>6</b>	H	Ph	H	1.09	-2.79	<i>-1.16</i>							
<b>7</b>	Me	Ph	H	1.12	-2.38	<i>-1.61</i>			-2.38	<i>-1.83</i>			
<b>8</b>	<sup>t</sup> Bu	Ph	H	1.15	-1.75	-1.45	-1.60	300	-1.99	-1.82	-1.90	170	300
<b>9</b>	Me <sub>3</sub> Si	Ph	H	1.25	-2.09	-1.58	-1.84	510	-2.09	-1.91	-2.00	180	160
<b>10</b>	H	Ph	Me	0.70	-2.88	<i>-1.67</i>							
<b>13</b>	H	<sup>i</sup> Pr	H	0.75	-2.89	<i>-1.48</i>							
<b>14</b>	Me <sub>3</sub> Si	<sup>i</sup> Pr	H	1.11	-1.96	-1.30	-1.63	670	-1.96	-1.73	-1.85	230	220
<b>15</b>	Me	H	H	0.96	-2.96	<i>-1.64</i>			-2.96	<i>-1.86</i>			

[a] Irreversible wave [b] Value in italics correspond to anodic wave of the species formed on rearrangement, reaction or decomposition of the initial reduced species

Differences of 330 and 300 mV between the two one-electron reduction waves for the butyl derivatives **4** and **8** in acetonitrile indicate the radical monoanions to be stable with respect to disproportionation ( $K_c \sim 1.2 - 3.8 \times 10^5$ ). The phenyl and silyl derivatives have smaller differences of 120 (**3**), 170 (**5**), 160 (**9**) and 220 (**14**) mV. The reported value for diphenyl-*ortho*-carborane in acetonitrile is 170 mV ( $K_c \sim 750$ )<sup>8</sup> so the radical anion for the phenyl derivative **3** is less stable but the radical anions for the butyl derivatives are more stable with respect to diphenyl-*ortho*-carborane and to the disproportionation into the dianion and neutral species. It is interesting to note that the electron-donating *tert*-butyl group facilitates radical anion stability more than the more electron-withdrawing phenyl group. It is presumed here that steric effects on the C1-C2 bond length of the carborane are more important for the stabilities of radical anions derived from diazaborolyl-*ortho*-carboranes than electronic effects.

### Spectroelectrochemistry

In view of our cyclic voltammetric results, compounds **3**, **4** and **5** were selected for the identification of their stable monoanions and dianions using spectroelectrochemical (and computational) methods. Figure 5 shows the IR spectra in the region between 1600 and 2800  $\text{cm}^{-1}$  and Table 5 lists the band maxima of the  $\nu(\text{BH})$ -vibrations of the monoanions and dianions on electrochemical reductions of **3**, **4** and **5**. Given the similarities between the IR spectra for the monoanions and the reported IR spectrum of the diphenyl-*ortho*-carborane radical monoanion,<sup>8</sup> these species have closely related cluster geometries with ‘free electrons’ located in the cages.



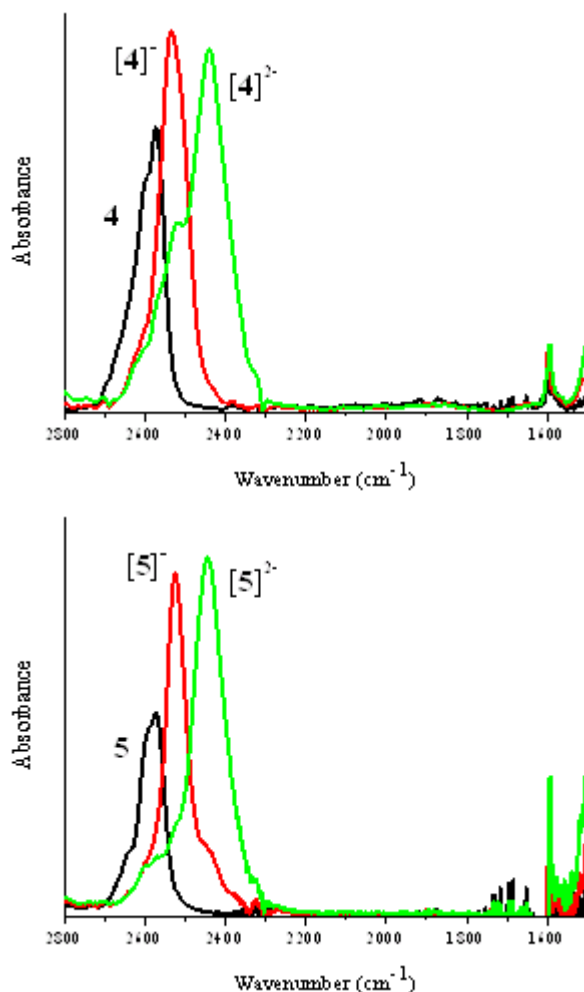


Figure 5. IR spectra for **3**, **4** and **5** and their mono- and dianions in the region 1600-2800  $\text{cm}^{-1}$  in an OTTLE cell (DCM, 0.1 M  ${}^n\text{Bu}_4\text{NPF}_6$ ).

The strong bands of the B-H stretching modes are shifted from 2675-2577  $\text{cm}^{-1}$  for the neutral species to 2541-2528  $\text{cm}^{-1}$  for the monoanions. Further reductions to the dianions led to  $\nu(\text{BH})$ -bands of 2451-2441  $\text{cm}^{-1}$  which are shifted from the B-H bands for the monoanions by 80-100  $\text{cm}^{-1}$ . In the case of the phenyl derivative **3**, the band assigned to the aromatic C-C stretch of the phenyl group is not significantly shifted on reduction with values between 1579 and 1589  $\text{cm}^{-1}$  but its band intensity increases on going from the neutral species via the radical anion to the dianion as shown in Figure 5.

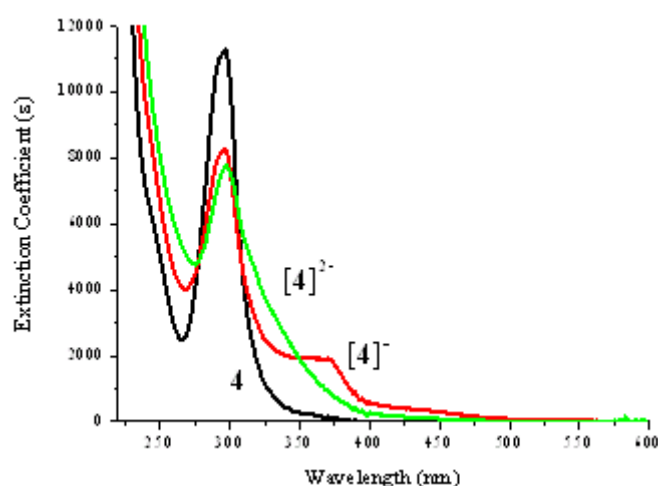
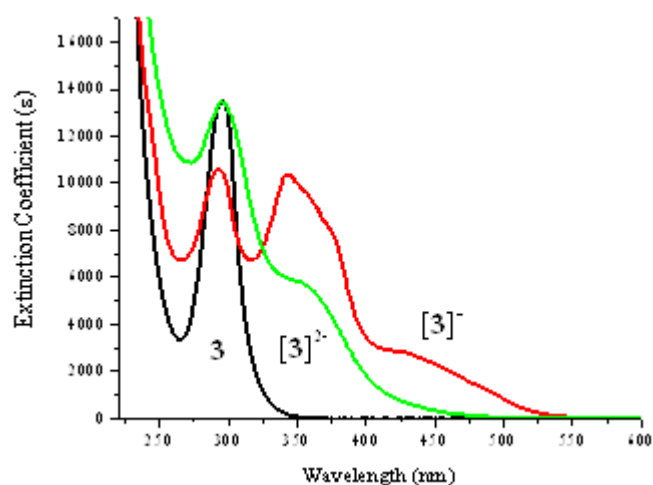
Table 5. IR data for  $[\mathbf{3}]^{n-}$ ,  $[\mathbf{4}]^{n-}$  and  $[\mathbf{5}]^{n-}$  ( $n = 0, -1, -2$ ) in 0.1 M  ${}^n\text{Bu}_4\text{NPF}_6$  DCM solutions.

	$n$	B-H stretch / $\text{cm}^{-1}$	Phenyl ring CC stretch / $\text{cm}^{-1}$
$[\mathbf{3}]^{n-}$	0	2675 (w), 2598 (m), 2580 (m)	1589 (w)
	1	2536 (s)	1579 (m)
	2	2451 (s)	1587 (s)
$[\mathbf{4}]^{n-}$	0	2536 (s), 2602 (m), 2577 (m)	

	1	2541 (s)
	2	2525 (sh), 2441 (s)
[5] <sup>0</sup>	0	2645 (w), 2595 (m), 2577 (m)
	1	2528 (s)
	2	2448 (s)

---

UV-visible spectra of the colourless compounds **3**, **4** and **5** display bands at 293-298 nm corresponding to local  $\pi - \pi^*$  transitions at the borolyl groups (Figure 6 and Table 6). Electrochemical reductions of these neutral species gave spectral profiles with several bands observed corresponding to the radical monoanions. Weak lowest-energy bands are found at 433-442 nm along with more intense bands at 340-370 nm. Further reductions gave spectra with broad bands between 300 and 400 nm corresponding to the dianions. The ill-defined spectra of the dianions were deconvoluted by Gaussian curve analyses with the lowest energy bands estimated at 382 – 400 nm.



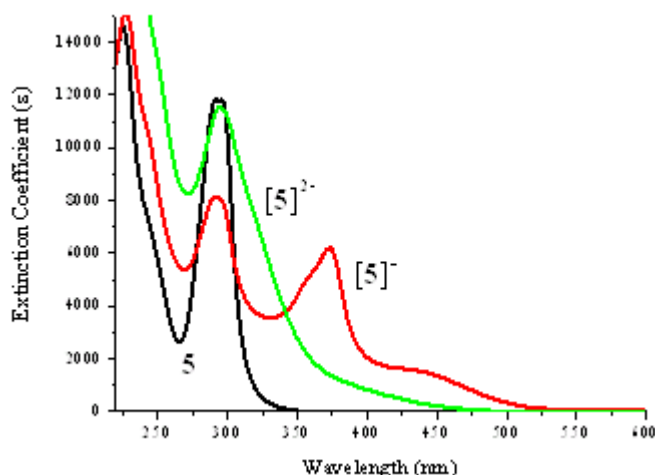


Figure 6. UV spectra for **3**, **4** and **5** and their mono and dianion species in an OTTLE cell (DCM, 0.1 M  $n\text{Bu}_4\text{NPF}_6$ ).

Table 6. UV-visible data for  $[\mathbf{3}]^{n-}$ ,  $[\mathbf{4}]^{n-}$  and  $[\mathbf{5}]^{n-}$  ( $n = 0, -1, -2$ ) in 0.1 M  $n\text{Bu}_4\text{NPF}_6$  DCM solutions.

	n	wavelength / nm (extinction coefficient $\epsilon / \text{M}^{-1}\text{cm}^{-1}$ )
$[\mathbf{3}]^{n-}$	0	297 (13500)
	1	441 (2600), 377 (7700), 362 (9100), 347 (10200), 295 (10500)
	2	400 (1200), 375 (3200), 355 (4300), 336 (4700), 318 (6500), 304 (9600), 291 (11000)
$[\mathbf{4}]^{n-}$	0	298 (11000), 296 (11300)
	1	433 (400), 372 (1900), 358 (1900), 345 (2000), 297 (8300), 292 (8100)
	2	382 (400), 364 (1000), 345 (1600), 329 (2400), 313 (4000), 298 (7000)
$[\mathbf{5}]^{n-}$	0	297 (11700), 293 (11800)
	1	442 (1300), 375 (6000), 361 (5300), 297 (7900), 292 (8100)
	2	400 (800), 370 (1200), 350 (2000), 331 (4200), 314 (6500), 300 (8400), 288 (7700)

## Geometry and MO Computations

### *Neutral species*

The optimised geometries of the neutral species **8-13** and **15** at B3LYP/6-31G\* are in good agreement with geometries determined experimentally. Comparison with computed and experimental data reported for **1-7** revealed one unusual difference as shown in Table 7. In the reported optimised geometry **4** has a C1-C2 bond length of 1.820 Å whereas in the optimised geometry for **8** a C1-C2 bond length of 1.765 Å was calculated. The experimentally determined C1-C2 bonds for **4** and **8** are similar at 1.756(1) Å and 1.750(2) Å, respectively (Table 1). Compounds **4** and **8** differ only in the Et and Ph substituents attached to the nitrogens of the borolyl group.

Table 7. Selected calculated geometric parameters and comparison between computed and observed MO energies for **1-15**.

	R <sup>1</sup>		C1-C2 (calc)	LUMO Energy Obs (V) <sup>[a]</sup>	LUMO Energy Calc (eV)	LUMO Type	HOMO Energy Obs (V) <sup>[b]</sup>	HOMO Energy Calc (eV)
<b>1</b>	H	$\psi = 13.9$	1.656	-2.64	-0.66	$\pi^*B$	-5.67	-5.87
		$\psi = 91.8$	1.676		-0.71	$\pi^*B$		-5.89
<b>2</b>	Me		1.714	-2.87	-0.85	$\pi^*B$	-5.84	-5.89
<b>3</b>	Ph		1.764	-3.22	-1.31	$\pi^*(\text{phenyl})$	-5.77	-5.78
<b>4</b>	<sup>t</sup> Bu	<b>4A</b> $\theta = 11.4$	1.820	-3.24	-1.12	$\pi^*B$	-5.78	-5.79
		<b>4B</b> $\theta = 58.0$	1.764		-0.82	$\pi^*B$		-5.84
<b>5</b>	Me <sub>3</sub> Si		1.750	-3.15	-0.85	$\pi^*B$	-5.82	-5.82
<b>6</b>	H	$\psi = 5.5$	1.659	-2.82	-0.74	$\pi^*(\text{phenyl})$	-5.89	-5.93
		$\psi = 90.1$	1.664		-0.63	$\pi^*B$		-5.96
<b>7</b>	Me		1.692	-2.80	-0.68	$\pi^*B$	-5.92	-5.95
<b>8</b>	<sup>t</sup> Bu	$\theta = 26.1$	1.765	-3.20	-0.77	$\pi^*B$	-5.95	-5.87
<b>9</b>	Me <sub>3</sub> Si		1.729	-2.96	-0.70	$\pi^*B$	-6.05	-5.91
<b>10</b>	H	$\psi = 1.8$	1.657	-2.53	-0.70	$\pi^*(\text{phenyl})$	-5.50	-5.66
		$\psi = 89.6$	1.665	-2.53	-0.55	$\pi^*B$	-5.50	-5.69
<b>11</b>	<sup>t</sup> Bu	$\theta = 29.4$	1.766	-2.88 <sup>[c]</sup>	-0.71	$\pi^*B$	-5.76 <sup>[c]</sup>	-5.61
<b>12</b>	Me <sub>3</sub> Si		1.730	-2.74 <sup>[c]</sup>	-0.63	$\pi^*B$	-6.11 <sup>[c]</sup>	-5.64
<b>13</b>	H	$\psi = 14.3$	1.664	-2.61	-0.66	$\pi^*B$	-5.55	-5.83
		$\psi = 88.8$	1.686		-0.73	$\pi^*B$		-5.85
<b>14</b>	Me <sub>3</sub> Si		1.761	-3.17	-0.89	$\pi^*B$	-5.91	-5.78
<b>15</b>	Me		1.685	-2.50	-0.72	$\pi^*B$	-5.76	-6.03

[a] Data from Table 4 using  $E(\text{MO}) = -E^{\text{a}}(\text{Ox}) - 4.8 \text{ V}$  with the FcH<sup>+</sup>/FcH couple at -4.8 V; [b] Data from Table 4 using  $E(\text{MO}) = -E^{\text{c}}(\text{Red1}) - 4.8 \text{ V}$ . [c] Data from Table 3.

The torsion angles C1-C2-C22-C23 ( $\theta$ , Figure 2) were considered to study the influence of the *tert*-butyl group rotation on the geometries for **4** and **8**. Figure S33 shows the total energies and the C1-C2 bond length with the angle  $\theta$  constrained at 5 degree intervals for **4** and **8**. Two minima were found for **4** and such conformers i.e. **4A** and **4B** were indeed observed in the crystal of **4**. Only one minimum was located for **8** and this conformer was determined by X-ray crystallography. The effect of the *tert*-butyl group on both geometries is intriguing with C1-C2 bond lengths varying from 1.76 to 1.83 Å for **4** and from 1.76 to 1.80 Å for **8** and with low rotation barriers of 0.6 kcal·mol<sup>-1</sup> for **4** and 1.0 kcal·mol<sup>-1</sup> for **8**. These C1-C2 bond length variations of 0.07 and 0.04 Å are larger than those of 0.01-0.03 Å computed for the rotations of a borolyl,<sup>16</sup> phenyl<sup>28</sup> or *tert*-butyl<sup>29</sup> group in C-monosubstituted carboranes. The combined steric congestion and mutual orientations of the *tert*-butyl and diazaborolyl groups influence the C1-C2 distance considerably.

Comparison of the bonds for the optimised geometries **4A**, **4B** and the experimental geometry of **4** listed in Table 8 reveals very good agreement between **4B** and **4** for all bonds whereas the agreement between **4A** and **4** is good except for the C1-C2 bond difference of 0.06 Å. Apart from the sensitive C1-C2 bond lengths listed in Table 7, similar bond lengths in the optimised geometry of **4B** are observed in the optimised geometries of the neutral compounds **1-3** and **5-15**.

Table 8. Comparison of selected bond lengths (Å) in the experimental geometry for **4** and the optimised geometries **4A**, **4B**,  $[\mathbf{4}]^-$ ,  $\mathbf{4} S_1$  (CT) and  $[\mathbf{4}]^{2-}$ .

Bond	<b>4</b>	<b>4A</b>	<b>4B</b>	$[\mathbf{4}]^-$	$\mathbf{4} S_1$ (CT)	$[\mathbf{4}]^{2-}$
C1-C2	1.7564(12)	1.820	1.764	2.445	2.420	2.991
C1-B3	1.7318(13)	1.729	1.730	1.759	1.693	2.686
C1-B6	1.7255(13)	1.724	1.726	1.761	1.689	1.555
C1-B4	1.7136(14)	1.699	1.719	1.635	1.636	1.618
C1-B5	1.7155(13)	1.699	1.719	1.635	1.637	1.617
C2-B3	1.7214(14)	1.713	1.729	1.707	1.759	1.527
C2-B6	1.7249(14)	1.720	1.729	1.705	1.762	2.640
C2-B7	1.7224(14)	1.709	1.719	1.641	1.616	1.617
C2-B11	1.7231(14)	1.717	1.721	1.642	1.615	1.616
C1-B2	1.6058(13)	1.610	1.615	1.548	1.589	1.517
C2-C22	1.5726(13)	1.581	1.585	1.550	1.540	1.540
N1-B2	1.4411(12)	1.446	1.450	1.462	1.470	1.481
N3-B2	1.4387(12)	1.448	1.447	1.462	1.474	1.476
N1-C9	1.3992(11)	1.401	1.401	1.391	1.374	1.382
N3-C8	1.3985(11)	1.400	1.401	1.391	1.371	1.395
C8-C9	1.4013(13)	1.408	1.408	1.418	1.442	1.428
C4-C9	1.3929(12)	1.396	1.396	1.394	1.402	1.394
C7-C8	1.3951(13)	1.396	1.396	1.394	1.399	1.395
C4-C5	1.3963(14)	1.397	1.397	1.402	1.388	1.407
C6-C7	1.3956(14)	1.397	1.397	1.402	1.390	1.407
C5-C6	1.3916(15)	1.399	1.399	1.396	1.419	1.394

While C-diazaborolyl-*ortho*-carboranes can be derived from benzodiazaborolyl groups with  $R^2 = \text{H, Et, } ^i\text{Pr or Ph}$  (Scheme 5), carboranes with N-mesityl or N-*tert*-butyl substituents are still elusive. Optimized geometries on these molecules revealed a highly distorted borolyl group for  $R^2 = ^t\text{Bu}$  and a borolyl group with little distortion for  $R^2 = \text{Mes}$ . This suggests severe steric hindrance in the case of *tert*-butyl groups at nitrogens preventing formation of the C-diazaborolyl-*ortho*-carborane and indeed notable distortions are present in the optimised geometry of the hypothetical bromoborole precursor **20**. The *ortho*-methyl groups in the mesityl groups may obstruct bond formation between the carborane anion and the boron atom of the fused ring system thus inhibiting the synthesis of the C-diazaborolyl-*ortho*-carborane with mesityl groups at nitrogens.

The optimised geometry of the carborane **31** with the  $\text{BBr}_2$  group at a cage carbon, which was not structurally characterised, gave calculated  $^{11}\text{B}$  GIAO-NMR data in good agreement with observed  $^{11}\text{B}$  NMR data where the peak for the three-coordinate boron is at 56.8 ppm. Comparison of the optimised geometry **31** with the optimised

geometry for the closely related benzodiazaborolyl carborane **15** reveals very similar C1-C2 and B2-C1 bond lengths for **31** (1.587; 1.679 Å) and **15** (1.581; 1.685 Å). Thus, both Br<sub>2</sub>B- and C<sub>6</sub>H<sub>4</sub>(NH)<sub>2</sub>B- groups exert similar structural effects on the carborane cluster.

As previously reported<sup>16</sup> earlier for compounds **1-7**, the HOMO is the  $\pi$ (borolyl) orbital whereas the LUMO may be the  $\pi^*$ B or a  $\pi^*$ (phenyl) orbital. HOMO and LUMO of **4B** are depicted in Figure 7. Table 7 lists the calculated LUMO and HOMO energies for **1-15** and compares them with the oxidation and reduction potentials obtained from CV data. Strictly speaking, observed half-wave oxidation and reduction potentials should be used for comparison but such values are not available for most compounds here. Therefore anodic oxidation and cathodic reduction potentials are used here for comparison. The agreement between the experimental oxidation potentials and the HOMO energies is reasonable. The observed reduction potentials, on the other hand, are in poor agreement with the calculated LUMO energies in the sense that there is no obvious trend between the two sets of values. For example, the computed LUMO energies for **2** and **5** are identical but the observed reduction potentials differ by 0.28 V. Here the predicted LUMO energies are thus poor guides for the estimation of the reduction potentials of disubstituted-*ortho*-carboranes. A better correlation between measured reduction potentials and C1-C2 bond lengths (experimental or computed) is shown in Table 7.

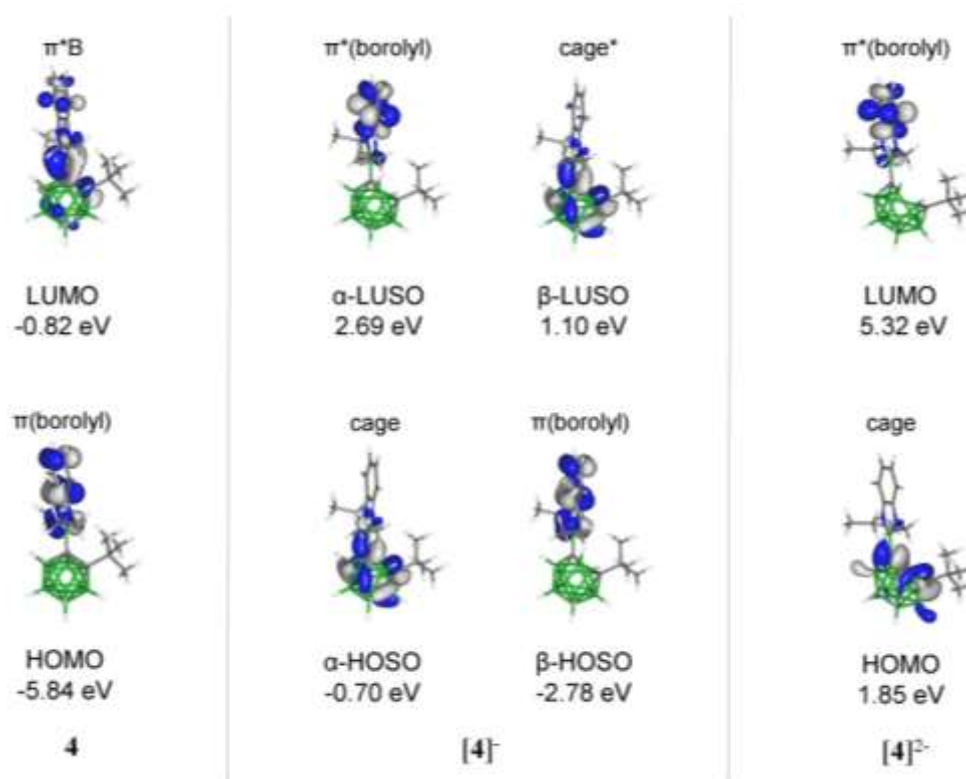


Figure 7. Selected molecular orbitals for **4**, **[4]<sup>-</sup>** and **[4]<sup>2-</sup>**.

The LUMO energy for **4** depends on the two conformers (minima) with -1.12 eV for **4A** and -0.82 eV for **4B**. The cage contributions to the LUMOs are 67% for **4A** and 51% for **4B** and suggest that an increase the C1-C2 bond results in an increase of the

cage contribution to the LUMO. This, in turn, could facilitate the one-electron reduction of the cluster.

### *Monoanions*

The optimised geometry of the monoanion  $[4]^-$  is shown here as a representative example for stable monoanion radical anions from **3**, **4**, **5**, **8**, **9**, **11**, **12** and **14** based on their CV data. The C1-C2 bond distances for the eight monoanions range from 2.425 Å [**3** $^-$ ] to 2.445 Å for  $[4]^-$  as shown in [Table S8](#). Selected bond lengths for the monoanion  $[4]^-$  are listed in Table 8 using the atom numbering given in Figure 2. The cluster geometry for  $[4]^-$  is clearly more distorted with a C1-C2 bond elongated in comparison to its neutral species **4** whereas the borolyl group in  $[4]^-$  resembles the borolyl group in **4**. The ‘free electron’ is thus located in the cage and the anion  $[4]^-$  has a  $2n+3$  skeletal electron count.

Comparison of selected bond lengths between the monoanion  $[4]^-$  and the excited state  $4S_1(\text{CT})$  geometries shows similarities in the cluster geometries. The C1-C2 distances are similar at 2.45 Å for  $[4]^-$  and 2.42 Å for the excited state  $4S_1(\text{CT})$ . The borolyl group inevitably acts as a ‘donor’ in the monoanion and as an ‘acceptor’ in the excited state thus closer examination of the clusters reveals essentially identical geometries whereby the ‘donor’ group at the carbon atom lengthens the B3/6-C bond i.e. B3/6-C1 of 1.76 Å for  $[4]^-$  and B3/6-C2 of 1.76 Å for  $4S_1(\text{CT})$ . Thus data on carborane monoanion radicals could be related to the excited state geometries of such carboranes which are responsible for the low-energy emissions observed here and elsewhere.

The ‘free’ electron in the monoanion radical is located in the cage based on open-shell electronic structure calculations where the highest singly occupied orbital, HOSO- $\alpha$ , represents the ‘free’ electron for the monoanion  $[4]^-$  in Figure 7. The HOSO- $\alpha$ , which is considered as the singly occupied molecular orbital SOMO, for  $[4]^-$  has 87% cage character and thus 36% more than the LUMO of the neutral species **4B**. It seems likely that addition of an electron to the neutral species goes initially to the  $\pi^*B$  orbital and the C1-C2 bond then elongates to accommodate the ‘free’ electron into the cage. This geometrical rearrangement may be the cause of the slow electron transfer process observed in the CV data for **4**. This process also applies to other carboranes, **5**, **8**, **9**, **11**, **12** and **14**, with <sup>t</sup>Bu or Me<sub>3</sub>Si groups. A different situation is given for **3** where the LUMO is located at the phenyl group. In this case, the electron initially goes to the  $\pi^*(\text{phenyl})$  orbital on reduction followed by rearrangement of the cage. This route is also likely in diphenyl-*ortho*-carborane (Figure 1) where slow electron transfer is also evident for the first reduction wave by detailed CV studies.<sup>8</sup>

### *Dianion species*

At least six different geometries for the *nido*-12-vertex carboranes are described.<sup>30</sup> According to quantum chemical calculations, the most stable geometries of the dianions **3**, **4**, **5**, **8**, **9**, **11**, **12** and **14** have C-C separations ranging from 2.944 Å [**9**]<sup>2-</sup> to 2.991 Å for  $[4]^{2-}$  ([Table S8](#)). They are similar to experimentally determined C-C distances in *nido*-12-vertex carboranes ([Table S9](#)).<sup>31</sup> Moreover calculated distances C1...B3 and C2...B6 (2.582 - 2.686 Å) are well comparable to experimentally obtained data (2.485 - 2.743 Å). Pertinent computed bond lengths for  $[4]^{2-}$ , which was selected as a representative for the dianions here, are collected in Table 8. The bonding parameters within the diazaborolyl fragments of  $[4]^-$  and  $[4]^{2-}$  are similar,

whereas changes in the cluster are obvious. Thus, distances C1-B3 and C2-B6 are elongated by 0.93 Å and the bond length C1-C2 increased by 0.55 Å. Obviously the second electron upon reduction of [4]<sup>-</sup> to [4]<sup>2-</sup> is accommodated in the cluster. The HOMO of dianion [4]<sup>2-</sup> has 90% cage character, whereas the LUMO is located at the C<sub>6</sub>H<sub>4</sub>-part of the benzodiazaborolyl substituent (Figure 7). From the similar geometries of [4]<sup>2-</sup> and [4]<sup>-</sup> and the natures of the HOMO in [4]<sup>2-</sup> and the SOMO [4]<sup>-</sup> one might expect a rapid electron transfer between the two species, which is underlined by the CV data presented earlier.

### Infrared and UV-Visible Computations

Selected data obtained by TD-DFT calculations for **3**, **4** and **5** and their anions and the corresponding experimental infrared- and UV-visible-data are listed in Table 9. In all cases excellent agreement between observed and computed IR-frequencies reflect the substantial shifts of the B-H stretching modes on sequential one-electron reduction (for simulated IR spectra of **3-5** and their anions see Figure S35).

TD-DFT data on the nine species are also in broad agreement with the observed low-energy bands. The relevant orbitals discussed here are shown in Figure 7 for [4]<sup>n-</sup> (n = 0, -1, -2) where similar orbitals are found for [3]<sup>n-</sup> and [5]<sup>n-</sup> analogues. In the neutral species, the strong bands observed at 4.19 eV correspond to HOMO > LUMO transitions ( $\pi(\text{borolyl}) > \pi\text{B}^*$ ) as reported elsewhere for **3-5**. The weak lowest energy bands observed for the three monoanionic radicals are assigned to  $\alpha\text{-HOSO} > \alpha\text{-LUSO}$  transitions which are largely cage to  $\pi^*(\text{borolyl})$  and thus charge-transfer in nature. Higher energy bands at 3.0-3.3 eV in the UV spectra of the monoanions are assigned to  $\pi(\text{borolyl}) > \text{cage}^*$  transitions ( $\beta\text{-HOSO} > \beta\text{-LUSO}$ ). The lowest energy bands observed for the dianions are assigned to HOMO > LUMO transitions (cage >  $\pi^*(\text{borolyl})$ ).

Given the excellent agreements between observed and computed spectroscopic data for the monoanions and dianions of **3-5**, the optimised geometries for these anions are likely to be found experimentally. These anion geometries are also present for reduced carboranes **8**, **9**, **11**, **12** and **14** as these compounds gave CV data similar to **4** and **5**.

Table 9. Comparison of observed IR and UV-visible data with calculated frequency and TD-DFT data for [3]<sup>n-</sup>, [4]<sup>n-</sup> and [5]<sup>n-</sup> (n = 0, -1, -2).

	Obs (cm <sup>-1</sup> )	Calc (cm <sup>-1</sup> )	Vibrationtype	Obs (eV)	Calc (eV)	Osc. Str. <sup>[a]</sup>	Major orbital contributions (%)	Transition type
<b>3</b>	2580	2580	B-H stretch	4.19	4.68	0.2099	HOMO > LUMO+2 (68)	$\pi(\text{borolyl}) > \pi\text{B}^*$
	1589	1572	CC ring stretch					
[3] <sup>-</sup>	2536	2525	B-H stretch	2.81	2.74	0.0434	$\alpha\text{-HOSO} > \alpha\text{-LUSO}$ (87)	cage > $\pi^*(\text{borolyl})$
	1579	1573	CC ring stretch	3.29	2.99	0.0794	$\beta\text{-HOSO} > \beta\text{-LUSO}$ (84)	$\pi(\text{borolyl}) > \text{cage}^*$
[3] <sup>2-</sup>	2451	2420	B-H stretch	3.10	3.08	0.0892	HOMO > LUMO (70)	cage > $\pi^*(\text{borolyl})$
	1587	1564	CC ring stretch					
<b>4A</b>	2577	2580	B-H stretch	4.19	4.15	0.2586	HOMO > LUMO (70)	$\pi(\text{borolyl}) > \pi\text{B}^*$
<b>4B</b>	2577	2580	B-H stretch	4.19	4.49	0.3009	HOMO > LUMO (67)	$\pi(\text{borolyl}) > \pi\text{B}^*$
[4] <sup>-</sup>	2541	2508	B-H stretch	2.87	2.82	0.0453	$\alpha\text{-HOSO} > \alpha\text{-LUSO}$ (97)	cage > $\pi^*(\text{borolyl})$
				3.34	3.21	0.1488	$\beta\text{-HOSO} > \beta\text{-LUSO}$ (95)	$\pi(\text{borolyl}) > \text{cage}^*$
[4] <sup>2-</sup>	2441	2412	B-H stretch	3.25	3.00	0.0809	HOMO > LUMO (70)	cage > $\pi^*(\text{borolyl})$
<b>5</b>	2580	2580	B-H stretch	4.19	4.44	0.2726	HOMO > LUMO (69)	$\pi(\text{borolyl}) > \pi\text{B}^*$
[5] <sup>-</sup>	2528	2509	B-H stretch	2.81	2.86	0.0338	$\alpha\text{-HOSO} > \alpha\text{-LUSO}$ (95)	cage > $\pi^*(\text{borolyl})$
				3.31	3.16	0.1602	$\beta\text{-HOSO} > \beta\text{-LUSO}$ (95)	$\pi(\text{borolyl}) > \text{cage}^*$
[5] <sup>2-</sup>	2448	2412	B-H stretch	3.10	3.12	0.0871	HOMO > LUMO (70)	cage > $\pi^*(\text{borolyl})$

[a] Oscillation Strength.

## Conclusions

The family of C-benzodiazaborolyl-*ortho*-carboranes has been expanded by three new benzodiazaborolyl groups. While most derivatives were synthesized using the standard bromoborole - lithiocarborane synthetic route, two alternative protocols to new C-benzodiazaborolyl-*ortho*-carboranes were developed. Low-energy fluorescence emissions were observed in the solution- and solid-state for seven of the eight new compounds with Stokes shifts between 14100 and 21000  $\text{cm}^{-1}$  and quantum yields up to 70%.

All fifteen C-diazaborolyl-carboranes examined by CV studies reveal oxidation and reduction waves in acetonitrile solutions. While oxidations are centered at the electron-donating benzodiazaborolyl groups, the reductions occur at the electron-withdrawing carborane clusters. For the C-diazaborolyl-*ortho*-carboranes with a phenyl, *tert*-butyl or trimethylsilyl substituent at the second carbon ( $\text{R}^1$  in Figure 8), the reduction waves showed evidence of stable monoanionic radicals and dianions. The stabilities of these anions were supported by infrared and UV-visible spectroelectrochemical methods. The anions were cleanly transferred to their neutral precursors by oxidation.



Figure 8. Postulated geometries of the anions obtained by reduction of carboranes with  $\text{R}^1 = \text{Ph}$ ,  $^t\text{Bu}$  and  $\text{SiMe}_3$ .

The geometries of the radical anions with  $2n+3$  skeletal electron counts and the dianions (*nido*,  $2n+4$  skeletal electron count) were determined by computations (Figure 8). The computed frequencies of the B-H stretching vibrations and TD-DFT data from these optimised geometries were in very good agreement with the spectroelectrochemical data indicating that such geometries may also be formed experimentally.

Based on the electronic structure calculations of the three geometries in Figure 8, the first reduction process involves adding an electron to the boron atom with the empty p-orbital followed by rearrangement of the cluster which allows the formation of the stable radical anion. The cluster rearrangement is likely to be responsible for the slow electron transfer reflected by the CV traces for the first reduction process. This slow electron transfer process is strongly dependent on the solvent which is perhaps not surprising given that negative charge is transferred from the borolyl group to the cage during the rearrangement process. The second reduction step is a straightforward addition of the second electron to the carborane radical anion resulting in a fast electron transfer as inferred from the CV studies.

For C-diazaborolyl-*ortho*-carboranes with hydrogen or methyl groups at the adjacent cage carbon, the measured reduction potentials here demonstrate that they are considerably more difficult to reduce in comparison to those with phenyl, *tert*-butyl and trimethylsilyl groups. This is strongly related to the C1-C2 bond distances where experimental values are 1.656-1.686 Å for R<sup>1</sup> = H, Me and 1.701-1.756 Å for R<sup>1</sup> = Ph, <sup>t</sup>Bu, SiMe<sub>3</sub>. The C1-C2 separations in neutral *ortho*-carboranes are thus important parameters for the stabilization of 12-vertex geometries with 2n+3 skeletal electron counts.

The similarities in the optimised cluster geometries of the monoanions here and the charge transfer (CT) singlet excited states of their neutral species suggest a close relationship between the monoanion and the S<sub>1</sub>(CT) state in these diazaborolylcarboranes. Low-energy emissions were observed for C-benzodiazaborolyl-*ortho*-carboranes with R<sup>1</sup> = Ph, <sup>t</sup>Bu, SiMe<sub>3</sub> which are also those with long C1-C2 bond distances and with the stable 2n+3 monoanions.

## Experimental

### General

All manipulations were performed under an atmosphere of dry oxygen-free argon using Schlenk techniques. All solvents were dried by standard methods and freshly distilled prior to use. The compounds 2-bromo-1,3-diethyl-1,3,2-benzodiazaborole,<sup>17</sup> 2-bromo-1,3-diphenyl-1,3,2-benzodiazaborole (**16**),<sup>19</sup> 4,5-dimethyl-*N,N'*-diphenyl-*ortho*-phenylenediamine (**25**),<sup>32</sup> *N,N'*-dimesityl-*ortho*-phenylenediamine (**26**),<sup>33</sup> *N,N'*-di-*tert*-butyl-*ortho*-phenylenediamine(**28**),<sup>34</sup> 1-*tert*-butyl-1,2-dicarbododecaborane<sup>35</sup> and 1-trimethylsilyl-1,2-dicarbododecaborane<sup>35</sup> were prepared as described in the literature. Compounds **22**, **23**, **29**, 1,2-dicarbododecaborane and 1-methyl-1,2-dicarbododecaborane were purchased commercially. NMR spectra were recorded from solutions at room temperature on a Bruker Avance III 300, a Bruker AM Avance DRX500 (<sup>1</sup>H, <sup>11</sup>B, <sup>13</sup>C), a Bruker Avance III 500 and a Bruker Avance 400 Spectrometer (<sup>1</sup>H{<sup>11</sup>B}) with SiMe<sub>4</sub> (<sup>1</sup>H, <sup>13</sup>C) and BF<sub>3</sub>·OEt<sub>2</sub> (<sup>11</sup>B) as external standards. <sup>1</sup>H- and <sup>13</sup>C{<sup>1</sup>H}-NMR-spectra were calibrated on the solvent signal [CDCl<sub>3</sub>: 7.24 (<sup>1</sup>H), 77.16 (<sup>13</sup>C); C<sub>6</sub>D<sub>6</sub>: 7.15 (<sup>1</sup>H), 128.06 (<sup>13</sup>C)]. The expected broad <sup>13</sup>C peaks corresponding to the carbon atoms attached to the borole-boron atoms were not detected above the noise levels. Mass spectra were recorded with a VG Autospec sector field mass spectrometer (Micromass). See Supporting Information for a detailed description of the photophysical experiments, further spectroscopic data, <sup>1</sup>H,<sup>13</sup>C{<sup>1</sup>H} and <sup>11</sup>B{<sup>1</sup>H} NMR spectra of carboranes **8-15** and detailed synthetic procedures. Typical procedures for the syntheses of C-benzodiazaborolyl-*ortho*-carboranes and 2-bromo-1,3,2-benzodiazaboroles are described below.

### Synthesis of 2-(1',2'-dicarbododecaboran-1'-yl)-1,3-diphenyl-5,6-dimethyl-1,3,2-benzodiazaborole (**10**).

*n*-Butyllithium (1.6M in *n*-hexane, 4.00mL, 6.40mmol) was added to a chilled (0 °C) solution of *ortho*-carborane (0.87g, 6.03mmol) in diethyl ether (10mL). After stirring for 1.5 h at room temperature a solution of 2-bromo-1,3-diphenyl-5,6-dimethyl-1,3,2-benzodiazaborole **17**, (2.28g, 6.05mmol) in toluene (11mL) was added dropwise at 0 °C. After stirring for 19 h at room temperature the solvent was removed *in vacuo*. The residue was extracted with hot toluene (5 × 10mL) and the combined extracts were

evaporated to dryness. The remaining solid was crystallized from dichloromethane (27 mL) and washed with *n*-hexane (8 mL). Product **10** was obtained as a colourless solid. Yield: 1.87 g (70%). Found: C, 59.77; H, 6.63; N, 6.33%; C<sub>22</sub>H<sub>29</sub>B<sub>11</sub>N<sub>2</sub> requires C, 60.00, H, 6.64; N, 6.36%; <sup>1</sup>H-NMR (CDCl<sub>3</sub>): δ [ppm] = 0.9 - 3.0 (m, br, 10 H, BH), 2.15 (s, 6 H, CCH<sub>3</sub>), 2.99 (s, br, 1 H, cage CH), 6.30 (s, 2 H, H<sub>4,7</sub>), 7.30 (m, 4 H, H<sub>ortho</sub>), 7.51 (m, 6 H, H<sub>meta</sub>, H<sub>para</sub>); <sup>13</sup>C{<sup>1</sup>H}-NMR (CDCl<sub>3</sub>): δ [ppm] = 19.9 (s, CCH<sub>3</sub>), 58.3 (s, cage CH), 111.8 (s, C<sub>4,7</sub>), 128.6 (s, C<sub>para</sub>), 129.5 (s, C<sub>ortho</sub>), 129.6 (s, C<sub>5,6</sub>), 129.9 (s, C<sub>meta</sub>), 136.1 (s, C<sub>8,9</sub>), 139.0 (s, C<sub>ipso</sub>); <sup>11</sup>B{<sup>1</sup>H}-NMR (CDCl<sub>3</sub>): δ [ppm] = -12.8 (s), -11.0 (s), -7.9 (s), -2.2 (s), 0.2 (s) (polyhedral boron atoms), 23.2 (s, exopolyhedral boron atom); MS (EI): m/z = 440.4 (M<sup>+</sup>, 100%), 425.3 (M<sup>+</sup>-Me, 10%).

### Synthesis of 2-bromo-1,3-diphenyl-5,6-dimethyl-1,3,2-benzodiazaborole (17).

A solution of 4,5-dimethyl-*N,N'*-diphenyl-*o*-phenylenediamine (**25**), (5.58g, 19.35mmol) in chloroform (60mL) was dripped to a mixture of calcium hydride (3.26g, 77.45 mmol), borontribromide (2.20mL, 5.81g, 23.21mmol) and chloroform (60mL). After stirring for 21 h at ambient temperature the mixture was filtered and the filter-cake was washed with chloroform (30mL). The combined filtrates were freed from volatiles and the residue was purified by short-path distillation (5·10<sup>-2</sup> mbar) using a flame. Product **17** was obtained as a colourless solid. Yield: 6.68 g (92%). <sup>1</sup>H-NMR (CDCl<sub>3</sub>): δ [ppm] = 2.26 (s, 6 H, C<sub>6</sub>H<sub>2</sub>(CH<sub>3</sub>)<sub>2</sub>), 6.89 (s, 2 H, H<sub>4,7</sub>), 7.39 (tt, <sup>3</sup>J<sub>HH</sub> = 7.3Hz, <sup>4</sup>J<sub>HH</sub> = 1.2Hz, 2 H, H<sub>para</sub>), 7.45 (dd, <sup>3</sup>J<sub>HH</sub> = 8.4Hz, <sup>4</sup>J<sub>HH</sub> = 1.2Hz, 4 H, H<sub>ortho</sub>), 7.52 (m, 4 H, H<sub>meta</sub>); <sup>13</sup>C{<sup>1</sup>H}-NMR (CDCl<sub>3</sub>): δ [ppm] = 20.0 (s, C<sub>6</sub>H<sub>2</sub>(CH<sub>3</sub>)<sub>2</sub>), 111.6 (s, C<sub>4,7</sub>), 126.7 (s, C<sub>para</sub>), 127.3 (s, C<sub>ortho</sub>), 128.9 (s, C<sub>5,6</sub>), 129.4 (s, C<sub>meta</sub>), 135.2 (s, C<sub>8,9</sub>), 139.3 (s, C<sub>ipso</sub>); <sup>11</sup>B{<sup>1</sup>H}-NMR (CDCl<sub>3</sub>): δ [ppm] = 23.6 (s); MS (EI): m/z = 375.9 (M<sup>+</sup>, 100%), 360.9 (M<sup>+</sup>-Me, 38%).

### Photophysics

All experiments in solution were performed in quartz cuvettes of 10 × 10 mm (Hellma type 111-QS, suprasil, optical precision). Cyclohexane was used as received from commercial sources (p. a. quality), the other solvents were dried by standard methods prior to use. Sample concentrations varied from 20 to 70 μM according to their optical density.

Solid samples were prepared by vacuum sublimation on quartz plates (35 × 10 × 1 mm) using standard Schlenk equipment and conditions.

Absorption spectra were taken with a UV/VIS double-beam spectrometer (Shimadzu UV-2550), using the solvent as a reference. The setup used to acquire excitation-emission spectra (EES) was similar to that employed in commercial static fluorimeters. The output of a continuous Xe-lamp (75 W, LOT Oriel) was wavelength-separated by a first monochromator (Spectra Pro ARC-175, 1800 l/mm grating, Blaze 250 nm) and then used to irradiate a sample. The fluorescence was collected by mirror optics at right angles and imaged on the entrance slit of a second spectrometer while compensating astigmatism at the same time. The signal was detected by a back-thinned CCD camera (RoperScientific, 1024 × 256 pixels) in the exit plane of the spectrometer. The resulting images were spatially and spectrally resolved. As the next step, one averaged fluorescence spectrum was calculated from

the raw images and stored in the computer. This process was repeated for different excitation wavelengths. The result is a two-dimensional fluorescence pattern with the *y*-axis corresponding to the excitation, and the *x*-axis to the emission wavelength. The time to acquire a complete EES is typically less than 15 min. Post-processing of the EES includes subtraction of the dark current background, conversion of pixel to wavelength scales, and multiplication with a reference file to take the varying lamp intensity as well as grating and detection efficiency into account. The quantum yields were determined against POPOP (*p*-bis-5-phenyl-oxazolyl(2)-benzene) ( $\Phi = 0.93$ ) as the standard.

The solid-state fluorescence was measured by addition of an integrating sphere (Labsphere, coated with Spectralon,  $\varnothing$  12.5 cm) to the existing experimental setup. At the exit slit of the first monochromator the exciting light was transferred into a quartz fiber (LOT Oriel, LLB592). It passed a condenser lens and illuminated a 1 cm<sup>2</sup> area on the sample in the centre of the sphere. The emission and exciting light was imaged by a second quartz fiber on the entrance slit of the detection monochromator. The optics for correction of astigmatism was passed by the light on this way.

Post-processing of the spectra was done as described above. The experimental determination and calculation of quantum yields was performed according to the method described by Mello.<sup>36</sup>

Stokes shifts were calculated from excitation and emission maxima, which were extracted from spectra that were converted from wavelength to wavenumbers beforehand.

### X-ray Crystallography

Single crystals were coated with a layer of hydrocarbon oil and attached to a glass fiber. Crystallographic data were collected with Nonius Kappa CCD and Bruker KAPPA APEX II diffractometers with Mo-K $\alpha$  radiation (graphite monochromator,  $\lambda = 0.71073$  Å) and a Bruker AXS X8 Prospector Ultra with APEX II with Cu-K $\alpha$  radiation (graphite monochromator,  $\lambda = 1.54178$  Å) at 100 K. Crystallographic programs used for structure solution and refinement were from SHELX-97.<sup>37</sup> The structures were solved by direct methods and were refined by using full-matrix least squares on  $F^2$  of all unique reflections with anisotropic thermal parameters for all non-hydrogen atoms. All hydrogen atoms, except those of a disordered methyl group, were refined isotropically for **15**. For **8** - **13** only the hydrogen atoms bonded to (non-disordered) carborane units were refined isotropically, the other hydrogen atoms were refined using a riding model with  $U(H) = 1.5 U_{eq}$  for CH<sub>3</sub> groups and  $U(H) = 1.2 U_{eq}$  for all others. For **19** all hydrogen atoms were refined using this riding model. Crystallographic data for the compounds are listed in **Table S2**. CCDC-894654 (**8**), CCDC-894655 (**9**), CCDC-894656 (**10**), CCDC-894657 (**11**), CCDC-894658 (**12**), CCDC-894659 (**13**), CCDC-894660 (**15**) and CCDC-894661 (**19**) contain the supplementary crystallographic data for this paper. These data can be obtained free of charge from the Cambridge Crystallographic Data Centre via [www.ccdc.cam.ac.uk/data\\_request/cif](http://www.ccdc.cam.ac.uk/data_request/cif)

### Cyclovoltammetry

Electrochemical measurements (Autolab PG-STAT 30) were carried out using dry dichloromethane or acetonitrile solutions containing 0.1 M NBu<sub>4</sub>PF<sub>6</sub> electrolyte in a standard three-electrode cell using platinum (1 mm diameter disc) or glassy carbon (2 mm) working electrodes with platinum wires as counter and reference electrodes.

Potentials are reported using an internal ferrocenium/ferrocene couple ( $\text{FcH}^+/\text{FcH} = 0.0 \text{ V}$ ) as reference. All electrochemical experiments were carried out in a glove box at ambient temperature.

### Spectroelectrochemistry

Spectroelectrochemical experiments were performed at room temperature in an airtight optically transparent thin-layer electrochemical (OTTLE) cell equipped with Pt minigrid working and counter electrodes ( $32 \text{ wires cm}^{-1}$ ), Ag wire pseudo-reference electrode and  $\text{CaF}_2$  windows for a  $200 \mu\text{m}$  path-length solvent compartment.<sup>38</sup> The cell was positioned in the sample compartment of a Nicolet Avatar 6700 FT-IR spectrometer or a Perkin-Elmer Lambda-900 spectrophotometer. An initial potential was applied such that no electrochemical work was done. The applied potential was then increased in a small (50 - 100 mV) step and the system allowed to reach equilibrium, as determined by both the decrease in current flowing through the cell and the reproducibility of spectra vs time, before further increase in applied potential. When complete electrolysis had been achieved (as determined by the relative changes in the spectroscopic profile), the chemical reversibility was determined by back oxidation using a similar sequence of controlled potential steps. The controlled-potential electrolyses were carried out using an Autolab PG-STAT 30 potentiostat.

### Computations

DFT calculations were performed with the Gaussian03 and 09 programs,<sup>39</sup> at the B3LYP/6-31G\* level<sup>40</sup> of theory. Geometry optimizations were performed without any symmetry constraints, and frequency calculations on the resulting optimized geometries showed no imaginary frequencies. The computed frequencies were scaled by 0.95 for comparison with observed IR data.<sup>41</sup> Electronic transitions were calculated by the time-dependent DFT (TD-DFT<sup>42</sup>) method. The MO contributions were generated using the GaussSum package<sup>43</sup> and plotted using the GabEdit<sup>44</sup> package. Calculated  $^{11}\text{B}$  chemical shifts for **31** were carried out on the optimised geometry of **31** using the GIAO<sup>45</sup>-NMR method and referenced to  $\text{BF}_3 \cdot \text{OEt}_2$  with  $\delta(^{11}\text{B}) = 111.7 - \sigma(^{11}\text{B})$ . Calculated GIAO  $^{11}\text{B}$ -NMR for **31**:  $\delta$  [ppm] = -11.7 (B4,5), -11.4 (B3,6), -10.7 (B7,11), -9.5 (B8,10), -5.7 (B9), 1.5 (B12), 68.7 (exopolyhedral boron atom).

## References

1. R. N. Grimes, *Carboranes*, 2nd edition; Academic Press (Elsevier) New York 2011.
2. For other reviews on carboranes; see (a) B. P. Dash, R. Satapathy, J. A. Maguire, N. S. Hosmane, *New J. Chem.* **2011**, *35*, 1955-1972; (b) I. B. Sivaev, V. V. Bregadze, *Eur. J. Inorg. Chem.* **2009**, 1433-1450; (c) F. Issa, M. Kassiou, L. M. Rendina, *Chem Rev.* **2011**, *111*, 5701-5722; (d) M. Scholz, E. Hey-Hawkins, *Chem. Rev.* **2011**, *111*, 7035-7062; (e) J. F. Valliant, K. J. Guenther, A. S. King, P. Morel, P. Schaffer, O. O. Sogbein, K. A. Stephenson, *Coord. Chem. Rev.* **2002**, *232*, 173-230; (f) V. N. Kalinin, V. A. Ol'shevskaya, *Russ. Chem. Bull.* **2008**, *57*, 815-836; (g) A. F. Armstrong, J. F. Valliant, *Dalton Trans.* **2007**, 4240-4251; (h) V. I. Bregadze, *Chem. Rev.* **1992**, *92*, 209-223; (i) L. A. Leites, *Chem. Rev.* **1992**, *92*, 279-323; (j) T. J. Wedge, M. F. Hawthorne, *Coord. Chem. Rev.* **2003**, *240*, 111-128.
3. (a) K. Wade, *Chem. Commun.* **1971**, 792; (b) K. Wade, *Adv. Inorg. Chem. Radiochem.* **1976**, *18*, 1.
4. (a) L. I. Zakharkin, *Pure Appl. Chem.* **1972**, *29*, 513-526; (b) J.H. Morris, H.J. Gysling, D. Reed, *Chem. Rev.* **1985**, *85*, 51-76.
5. (a) A. V. Bukhtiarov, V. N. Golyshin, A. V. Lebedev, Y. G. Kudryavtsev, I. A. Rodnikov, L. I. Zakharkin, O. V. Kuz'min, *Doklady Akad. Nauk SSSR* **1989**, *304*, 879-882 (Russian; English translation **1989**, 45-48); (b) A. V. Lebedev, A. V. Buchtiarov, N. N. Golyshin, Y. G. Kudryatsev, I. Y. Lovchinovsky, L. N. Rozhkov, *Metalloorganischeskaya Khim.* **1991**, *4*, 426-432 (Russian; English version *Organomet. Chem. USSR* **1991**, *4*, 205-208); (c) A. V. Lebedev, A. V. Bukhtiarov, Y. G. Kudryavtsev, I. N. Rozhkov, *Metalloorganischeskaya Khim.* **1991**, *4*, 433-438 (Russian; English version *Organomet. Chem. USSR*, **1991**, *4*, 208-212); (d) F. Teixidor, J. Pedrajas, C. Viñas, *Inorg. Chem.* **1995**, *34*, 1726-1729.
6. (a) C. E. Willans, C. A. Kilner, M. A. Fox, *Chem. Eur. J.* **2010**, *16*, 10644-10648; (b) A. R. Popescu, A. D. Musteti, A. Ferrer-Ugalde, C. Viñas, R. Núñez, F. Teixidor, *Chem. Eur. J.* **2012**, *18*, 3174-3184.
7. (a) M. V. Yarosh, T. V. Baranova, V. L. Shirokii, A. A. Érdman, N. A. Maier, *Élektrokimiya*, **1993**, *29*, 921-922 (Russian; English version *Russ. J. Electrochem.* **1993**, *29*, 789-790); (b) M. V. Yarosh, T. V. Baranova, V. L. Shirokii, A. A. Érdman, N. A. Maier, *Élektrokimiya* **1994**, *30*, 406-408 (Russian; English version *Russ. J. Electrochem.* **1994**, *30*, 366-368).
8. M. A. Fox, C. Nervi, A. Crivello, P. J. Low, *Chem. Commun.* **2007**, 2372-2374.
9. (a) G. D. Mercer, J. Lang, R. Reed, F. R. Scholer, *Inorg. Chem.* **1975**, *14*, 761-763; (b) N. S. Hosmane, H. Zhang, J. A. Maguire, Y. Wang, T. Demissie, T. J. Colacot, M. B. Ezhova, K.-J. Lu, D. Zhu, T. G. Gray, S. C. Helfert, S. N. Hosmane, J. D. Collins, F. Baumann, W. Kaim, W. N. Lipscomb, *Organometallics* **2000**, *19*, 497-508; (c) X. Fu, H.-S. Chan, Z. Xie, *J. Am. Chem. Soc.* **2007**, *129*, 8964-8965.
10. K. Hosoi, S. Inagi, T. Kubo, T. Fuchigami, *Chem. Commun.* **2011**, *47*, 8632-8634.
11. M. A. Fox, C. Nervi, A. Crivello, A. S. Batsanov, J. A. K. Howard, K. Wade, P. J. Low, *J. Solid State Electrochem.* **2009**, *13*, 1483-1495.

12. H. Tricas, M. Colon, D. Ellis, S. A. Macgregor, D. McKay, G. M. Rosair, A. J. Welch, I. V. Glukhov, F. Rossi, F. Laschi, P. Zanello, *Dalton Trans.* **2011**, *40*, 4200-4211.
13. K.-R. Wee, W.-S. Han, D. W. Cho, S. Kwon, C. Pac, S. O. Kang, *Angew. Chem. Int. Ed.* **2012**, *51*, 2677-2680.
14. (a) K. Kokado, Y. Chujo, *Macromolecules* **2009**, *42*, 1418-1420; (b) J. J. Peterson, M. Werre, Y. C. Simon, E. B. Coughlin, K. R. Carter, *Macromolecules* **2009**, *42*, 8594-8598; (c) K. Kokado, Y. Tokoro, Y. Chujo, *Macromolecules* **2009**, *42*, 9238-9242; (d) K. Kokado, Y. Chujo, *Polym. J.* **2010**, *42*, 363-367; (e) K. Kokado, A. Nagai, Y. Chujo, *Tetrahedron Lett.* **2011**, *52*, 293-296; (f) K. Kokado, Y. Chujo, *Dalton Trans.* **2011**, *40*, 1919-1923; (g) K. Kokado, Y. Chujo, *J. Org. Chem.* **2011**, *76*, 316-319; (h) J. J. Peterson, A. R. Davis, M. Werre, E. B. Coughlin, K. R. Carter, *ACS Appl. Mater. Interfaces* **2011**, *3*, 1796-1799; (i) A. R. Davis, J. J. Peterson, K. R. Carter, *ACS Macro Lett.* **2012**, *1*, 469-472.
15. A. Ferrer-Ugalde, E. J. Juárez-Pérez, F. Teixidor, C. Viñas, R. Sillanpää, E. Pérez-Inestrosa, R. Núñez, *Chem. Eur. J.* **2012**, *18*, 544-553.
16. L. Weber, J. Kahlert, R. Brockhinke, L. Böhling, A. Brockhinke, H.-G. Stammler, B. Neumann, R. A. Harder, M. A. Fox, *Chem. Eur. J.* **2012**, *18*, 8347-8357.
17. L. Weber, H. B. Wartig, H.-G. Stammler, B. Neumann, *Z. Anorg. Allg. Chem.* **2001**, *627*, 2663-2668.
18. (a) L. Weber, D. Eickhoff, T. B. Marder, M. A. Fox, P. J. Low, A. D. Dwyer, D. J. Tozer, S. Schwedler, A. Brockhinke, H.-G. Stammler, B. Neumann, *Chem. Eur. J.* **2012**, *18*, 1369-1382; (b) L. Weber, V. Werner, M. A. Fox, T. B. Marder, S. Schwedler, A. Brockhinke, H.-G. Stammler, B. Neumann, *Dalton Trans.* **2009**, 1339-1351; (c) L. Weber, V. Werner, M. A. Fox, T. B. Marder, S. Schwedler, A. Brockhinke, H.-G. Stammler, B. Neumann, *Dalton Trans.* **2009**, 2823-2831; (d) L. Weber, D. Eickhoff, V. Werner, L. Böhling, S. Schwedler, A. Chrostowska, A. Dargelos, M. Maciejczyk, H.-G. Stammler, B. Neumann, *Dalton Trans.* **2011**, *40*, 4434-4446.
19. L. Weber, J. Halama, V. Werner, K. Hanke, L. Böhling, A. Chrostowska, A. Dargelos, M. Maciejczyk, A. L. Raza, H.-G. Stammler, B. Neumann, *Eur. J. Inorg. Chem.* **2010**, 5416-5425.
20. L. Weber, D. Eickhoff, J. Kahlert, L. Böhling, A. Brockhinke, H.-G. Stammler, B. Neumann, M. A. Fox, *Dalton Trans.* **2012**, *41*, 10328-10346.
21. (a) L. Weber, V. Werner, I. Domke, H.-G. Stammler, B. Neumann, *Dalton Trans.* **2006**, 3777-3784; (b) L. Weber, A. Penner, I. Domke, H.-G. Stammler, B. Neumann, *Z. Anorg. Allg. Chem.* **2007**, *633*, 563-569.
22. (a) S. Schwedler, D. Eickhoff, R. Brockhinke, D. Cherian, L. Weber, A. Brockhinke, *Phys. Chem. Chem. Phys.* **2011**, *13*, 9301-9310; (b) L. Weber, J. Halama, L. Böhling, A. Chrostowska, A. Dargelos, H.-G. Stammler, B. Neumann, *Eur. J. Inorg. Chem.* **2011**, 3091-3101.
23. R. Goetze, H. Nöth, *Chem. Ber.* **1976**, *109*, 3247-3249.
24. (a) T. Habereeder, H. Nöth, *Appl. Organomet. Chem.* **2003**, *17*, 525-538. (b) H. R. Morales, M. Pérez-Juárez, L. Cuéllar, L. Mendoza, H. Fernandez, R. Contreras, *Synth. Commun.* **1984**, *14*, 1213-1220.
25. M. A. Fox, A. K. Hughes, *Coord. Chem. Rev.* **2004**, *248*, 457-476.
26. K. M. Lee, J. O. Huh, T. Kim, Y. Do, M. H. Lee, *Dalton Trans.* **2011**, *40*, 11758-11764.

27. S. Maruyama, Y. Kawanishi, *J. Mater. Chem.* **2002**, *12*, 2245-2249.
28. E. S. Alekseyeva, M. A. Fox, J. A. K. Howard, J. A. H. MacBride, K. Wade, *Appl. Organomet. Chem.* **2003**, *17*, 499-508.
29. M. Tsuji, *J. Org. Chem.* **2004**, *69*, 4063-4074.
30. M. A. Fox, in *Comprehensive Organometallic Chemistry III*, eds. Crabtree, R. H. Mingos, D. M. P., Elsevier, Oxford, **2007**, vol 3, pp 49-112.
31. (a) T. L. Venable, R. B. Maynard, R. N. Grimes, *J. Am. Chem. Soc.* **1984**, *106*, 6187-6193; (b) J. T. Spencer, M. R. Pourian, R. J. Butcher, E. Sinn, R. N. Grimes, *Organometallics* **1987**, *6*, 335-343; (c) N. S. Hosmane, T. J. Colacot, H. Zhang, J. Yang, J. A. Maguire, Y. Wang, M. B. Ezhova, A. Franken, T. Demissie, K.-J. Lu, D. Zhu, J. L. C. Thomas, J. D. Collins, T. G. Gray, S. N. Hosmane, W. N. Lipscomb, *Organometallics* **1998**, *17*, 5294-5309; (d) G. Zi, H.-W. Li, Z. Xie, *Organometallics* **2002**, *21*, 5415-5427; (e) L. Deng, M.-S. Cheung, H.-S. Chen, Z. Xie, *Organometallics* **2005**, *24*, 6244-6249; (f) J. P. H. Charmant, M. F. Haddow, R. Mistry, N. C. Norman, A. G. Orpen, P. G. Pringle, *Dalton Trans.* **2008**, 1409-1411.
32. T. Wenderski, K. M. Light, D. Ogrin, S. G. Bott, C. J. Harlan, *Tetrahedron Lett.* **2004**, *45*, 6851-6853.
33. J. V. Dickschat, S. Urban, T. Pape, F. Glorius, F. E. Hahn, *Dalton Trans.* **2010**, *39*, 11519-11521.
34. D. M. Khramov, C. W. Bielawski, *J. Org. Chem.* **2007**, *72*, 9407-9417.
35. M. Tsuji, *J. Org. Chem.* **2003**, *68*, 9589-9597.
36. J. C. de Mello, H. F. Wittmann, R. H. Friend, *Adv. Mater.* **1997**, *9*, 230-232.
37. G. M. Sheldrick, *Acta Cryst.* **2008**, *A64*, 112-122.
38. M. Krejčík, M. Daněk, F. Hartl, *J. Electroanal. Chem.* **1991**, *317*, 179-187.
39. (a) Gaussian 03, Revision E.01, M. J. Frisch, G. W. Trucks, H. B. Schlegel, G. E. Scuseria, M. A. Robb, J. R. Cheeseman, J. A. Montgomery, Jr., T. Vreven, K. N. Kudin, J. C. Burant, J.M. Millam, S. S. Iyengar, J. Tomasi, V. Barone, B. Mennucci, M. Cossi, G. Scalmani, N. Rega, G. A. Petersson, H. Nakatsuji, M. Hada, M. Ehara, K. Toyota, R. Fukuda, J. Hasegawa, M. Ishida, T. Nakajima, Y. Honda, O. Kitao, H. Nakai, M. Klene, X. Li, J. E. Knox, H. P. Hratchian, J. B. Cross, V. Bakken, C. Adamo, J. Jaramillo, R. Gomperts, R. E. Stratmann, O. Yazyev, A. J. Austin, R. Cammi, C. Pomelli, J. W. Ochterski, P. Y. Ayala, K. Morokuma, G. A. Voth, P. Salvador, J. J. Dannenberg, V. G. Zakrzewski, S. Dapprich, A. D. Daniels, M. C. Strain, O. Farkas, D. K. Malick, A. D. Rabuck, K. Raghavachari, J. B. Foresman, J. V. Ortiz, Q. Cui, A. G. Baboul, S. Clifford, J. Cioslowski, B. B. Stefanov, G. Liu, A. Liashenko, P. Piskorz, I. Komaromi, R. L. Martin, D. J. Fox, T. Keith, M. A. Al-Laham, C. Y. Peng, A. Nanayakkara, M. Challacombe, P. M. W. Gill, B. Johnson, W. Chen, M. W. Wong, C. Gonzalez, and J. A. Pople, Gaussian, Inc., Wallingford CT, 2004. (b) Gaussian 09, Revision A.02, M. J. Frisch, G. W. Trucks, H. B. Schlegel, G. E. Scuseria, M. A. Robb, J. R. Cheeseman, G. Scalmani, V. Barone, B. Mennucci, G. A. Petersson, H. Nakatsuji, M. Caricato, X. Li, H. P. Hratchian, A. F. Izmaylov, J. Bloino, G. Zheng, J. L. Sonnenberg, M. Hada, M. Ehara, K. Toyota, R. Fukuda, J. Hasegawa, M. Ishida, T. Nakajima, Y. Honda, O. Kitao, H. Nakai, T. Vreven, Jr., J. A. Montgomery, J. E. Peralta, F. Ogliaro, M. Bearpark, J. J. Heyd, E. Brothers, K. N. Kudin, V. N. Staroverov, R. Kobayashi, J. Normand, K. Raghavachari, A. Rendell, J. C. Burant, S. S. Iyengar, J. Tomasi, M. Cossi, N. Rega, J. M. Millam, M. Klene, J. E. Knox, J. B. Cross, V. Bakken, C. Adamo, J.

- Jaramillo, R. Gomperts, R. E. Stratmann, O. Yazyev, A. J. Austin, R. Cammi, C. Pomelli, J. W. Ochterski, R. L. Martin, K. Morokuma, V. G. Zakrzewski, G. A. Voth, P. Salvador, J. J. Dannenberg, S. Dapprich, A. D. Daniels, O. Farkas, J. B. Foresman, J. V. Ortiz, J. Cioslowski, D. J. Fox, *Gaussian, Inc.*, Wallingford CT, **2009**.
40. (a) A. D. Becke, *J. Chem. Phys.* **1993**, *98*, 5648-5652; (b) C. Lee, W. Yang, R. G. Parr, *Phys. Rev. B* **1988**, *37*, 785-789; (c) G. A. Petersson, M. A. Al-Laham, *J. Chem. Phys.* **1991**, *94*, 6081-6090; (d) G. A. Petersson, A. Bennett, T. G. Tensfeldt, M. A. Al-Laham, W. A. Shirley, J. Mantzaris, *J. Chem. Phys.* **1988**, *89*, 2193-2218.
41. J. P. Merrick, D. Moran, L. Radom, *J. Phys. Chem. A* **2007**, *111*, 11683-11700.
42. E. Runge, E. K. U. Gross, *Phys. Rev. Lett.* **1984**, *52*, 997-1000.
43. N. M. O'Boyle, A. L. Tenderholt, K. M. Langner, *J. Comp. Chem.* **2008**, *29*, 839-845.
44. A. R. Allouche, *J. Comp. Chem.* **2011**, *32*, 174-182.
45. (a) R. Ditchfield, *Mol. Phys.* **1974**, *27*, 789-807; (b) C. M. Rohling, L. C. Allen, R. Ditchfield, *Chem. Phys.* **1984**, *87*, 9-15; (c) K. Wolinski, J. F. Hinton, P. Pulay, *J. Am. Chem. Soc.* **1990**, *112*, 8251-8260.